GEOLOGY FOR SOCIETY

SINCE 1858

GEOLOGICAL
SURVEY OF
NORWAY

· NGU ·

REPORT

Report no.: 2015.019	**ISSN: 0800-3416 (print)** **ISSN: 2387-3515 (online)**	**Grading:** Confidential until 01.06.2017

Title: Scenarios of microcontinent formation applied to the Jan Mayen microcontinent

Authors: Joya Tetreault and Susanne J.H. Buiter	**Client:** Det norske oljeselskap ASA
County:	**Commune:**
Map-sheet name (M=1:250.000)	**Map-sheet no. and -name (M=1:50.000)**
Deposit name and grid-reference:	**Number of pages:** 55 **Price (NOK):** 180,- **Map enclosures:**

Fieldwork carried out:	**Date of report:** 01.06.2015	**Project no.:** 347200	**Person responsible:**

Summary: The Jan Mayen microcontinent is a small, unique, crustal entity that was separated from the Norwegian and Greenland margins by two distinct rifting events. Seafloor spreading along the Aegir Ridge separated Jan Mayen (together with Greenland) from Norway by ca. 54 Ma. Cessation of seafloor spreading on the Aegir Ridge at ca. 30 Ma was more or less simultaneous with the onset of extension along the Kolbeinsey Ridge between Jan Mayen and Greenland. Break-up along the Kolbeinsey Ridge by ca. 23 or 20 Ma isolated the Jan Mayen microcontinent. Several scenarios have been put forward to explain the formation of microcontinents and continental fragments: (1) inherited faults or lateral inhomogeneities in lithospheric rheology that localise deformation in multiple locations, (2) strain localisation by serpentinization or magmatic underplating, (3) back-arc extension related to slab rollback, (4) local misalignment of rift axes, (5) multiphase rifting, and (6) magmatic influence of mantle plumes. We use geodynamic numerical experiments in 2-D and 3-D to test scenarios of microcontinent formation that are pertinent to the tectonic setting of Jan Mayen. We illustrate how these scenarios produce different topographic, structural, and heat flow signals. Our results demonstrate that inherited structural inhomogeneities can serve to focus the location of initial rifting on multiple rifts, but will not lead to crustal break-up in more than one location. Ultraslow extension, multiple stages of rifting, or a crustal rheological structure with a weak middle crust will all produce continental fragments, but not a microcontinent. This clearly illustrates that a second process is necessary to initiate rifting on the other side of a continental fragment once seafloor spreading is underway on one side, thus turning the fragment into a microcontinent. We invoke the influence of hot, molten plume material related to the Iceland Plume, which was at a location near the western edge of future Jan Mayen at approximately 40–30 Ma. In our 2-D numerical experiments, we show that a plume impacting on the lithosphere can re-initiate a failed rift and create a microcontinent. The melt migrating from the rising plume underplates the continental crust and induces break-up in the formerly failed rift at the expense of the initial successful rift. This scenario of microntinent formation explains a fast jump in rift location similar to what is deduced for Jan Mayen.

Keywords:	Jan Mayen	Microcontinent
Numerical models	Plume	Melt
Continental break-up		

CONTENTS

1. INTRODUCTION: SCENARIOS OF MICROCONTINENT FORMATION

Microcontinents, such as Jan Mayen and the Seychelles, are small, stretched pieces of continental crust that are surrounded by oceanic crust on all sides (*Fig. 1*) (Scrutton, 1966). This description separates microcontinents from continental fragments, such as Hatton Bank and Rockall Bank, which are still connected to the continental mainland by thinned crust or serpentinized mantle. Microcontinents have an average crustal thickness of 23–25 km (Tetreault and Buiter, 2014; 2015), which suggests that these regions have undergone moderate amounts of stretching in comparison with the average 41 km thickness of continental crust (Christensen and Mooney, 1995).
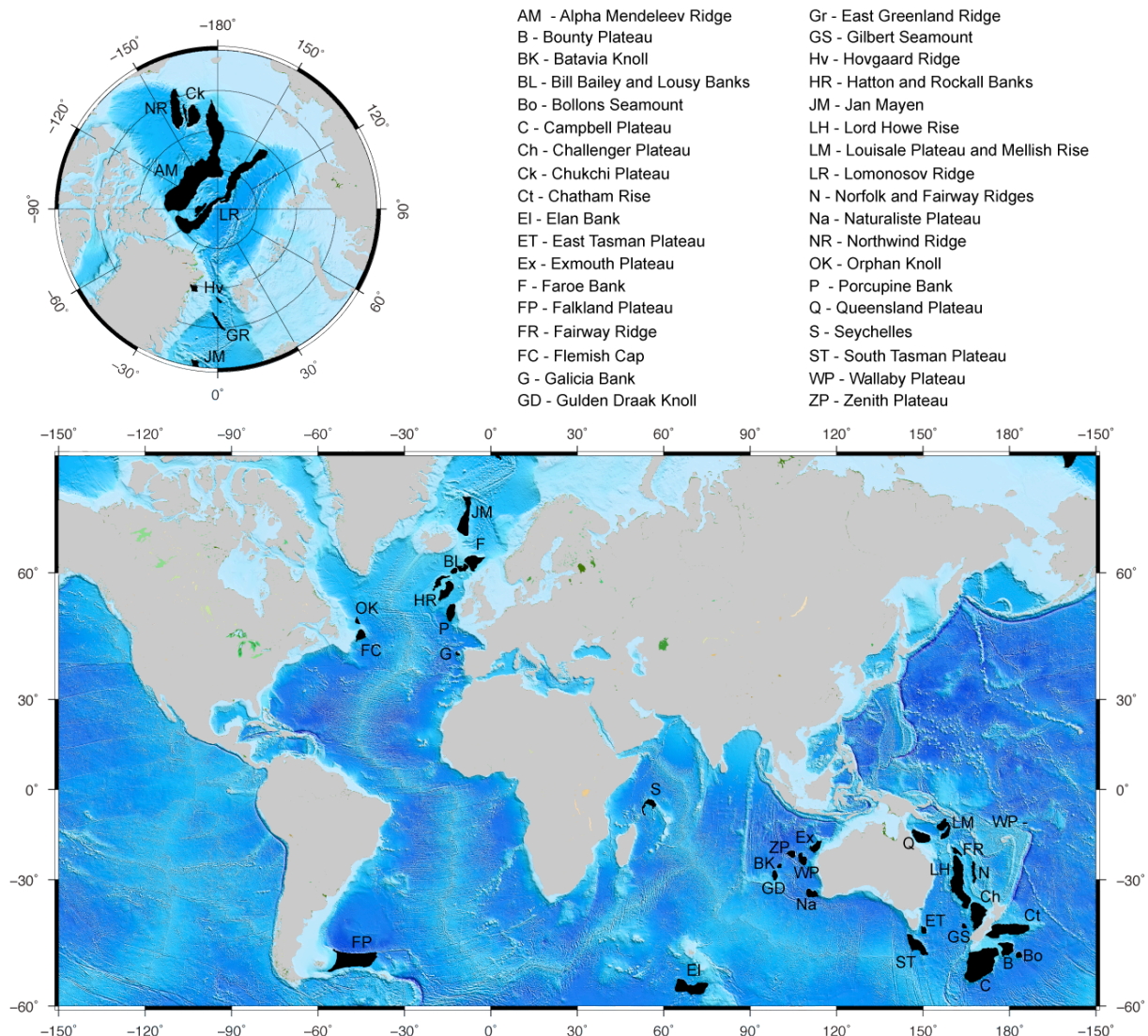
AM - Alpha Mendeleev Ridge	Gr - East Greenland Ridge
B - Bounty Plateau	GS - Gilbert Seamount
BK - Batavia Knoll	Hv - Hovgaard Ridge
BL - Bill Bailey and Lousy Banks	HR - Hatton and Rockall Banks
Bo - Bollons Seamount	JM - Jan Mayen
C - Campbell Plateau	LH - Lord Howe Rise
Ch - Challenger Plateau	LM - Louisale Plateau and Mellish Rise
Ck - Chukchi Plateau	LR - Lomonosov Ridge
Ct - Chatham Rise	N - Norfolk and Fairway Ridges
El - Elan Bank	Na - Naturaliste Plateau
ET - East Tasman Plateau	NR - Northwind Ridge
Ex - Exmouth Plateau	OK - Orphan Knoll
F - Faroe Bank	P - Porcupine Bank
FP - Falkland Plateau	Q - Queensland Plateau
FR - Fairway Ridge	S - Seychelles
FC - Flemish Cap	ST - South Tasman Plateau
G - Galicia Bank	WP - Wallaby Plateau
GD - Gulden Draak Knoll	ZP - Zenith Plateau

Figure 1*: Map of microcontinents and continental fragments. Modified from Tetreault and Buiter (2014).*

The formation of microcontinents poses an intriguing scenario of continental deformation because it requires strain localisation at different locations in an extending continent to occur either simultaneously or subsequently. This presents a mechanical challenge because of the innate physical difficulty in maintaining continental stretching in multiple locations or especially in initiating stretching at a new location once rifting and continental thinning has already rendered the crust in a nearby location thin and weak. This physical challenge has led to many different hypotheses for how microcontinents and continental fragments form:

1) Microcontinents could form by more-or-less simultaneous localisation of extension in regions of pre-existing weaknesses that are inherited from earlier continental collisions. Many continental rifts form on ancient sutures zones (Buiter and Torsvik, 2014). Because sutures can be several hundreds of kilometres wide, include deep-rooting thrusts, and juxtapose terranes of different lithologies and strengths, they offer multiple locations for localisation of continental extension. In fact, this mechanism leading to the localisation of deformation in multiple rifts has been used to account for the Mesozoic basins surrounding the continental fragments off of the Irish Margin (Shannon, 1991). Specifically, the Rockall, Hatton, and Faroe-Shetland basins and basement lineations in the Rockall and Hatton Banks run parallel to Caledonian trends (Naylor and Shannon, 1995). Also the interplay of inheritance with the evolution from moderate stretching, to thinning, and then to local exhumation of the continental lithosphere at passive margins may isolate continental ribbons (or continental fragments) (Péron-Pinvidic and Manatschal, 2010) (*Figs. 2, 3*). The first stages of extension result in overall stretching of the continental lithosphere. With ongoing extension, the thinning phase localises deformation along a few major faults at the borders of rheologically stronger blocks. This localisation will be aided by inherited structures (Péron-Pinvidic and Manatschal, 2010). In the exhumation phase, large detachment faults exhume lower crustal and mantle rocks. Due to rheological heterogeneities, not all regions of highly thinned crust or exhumed mantle will proceed to break-up and seafloor spreading, which may result in the isolation of continental fragments.

2) Several continental fragments and their surrounding basins are underlain by a seismic high-velocity layer, which is interpreted as either mafic underplating or serpentinised mantle. Examples are, among others, Seychelles, Mendeleev Ridge, Lousy Bank and Hatton Bank (Tetreault and Buiter, 2014) (*Fig. 4*). Serpentinization or underplating may create multiple weak zones in a wide rift region that may localise strain and thus aid microcontinent formation (Lundin and Doré, 2011; Armitage et al., 2011). However, serpentinization of mantle rocks starts in presence of water at temperatures of 300–500 °C constraining the process to depths of <10 km (Escartin et al., 1997; Mével, 2003; Hirth and Guillot, 2013). Therefore serpentinization is an unlikely factor in influencing crustal strength during the earlier stages of rifting. A structural review of the North Atlantic passive margins indicates that the high volumes of magma on the volcanic margins of the North Atlantic were emplaced at the latest stages of passive margin formation (Peron-Pinvidic et al., 2013). Because serpentinization and underplating occur relatively late in the rifting process, they cannot be the primary cause of strain localisation at multiple locations. Our numerical experiments confirm that while serpentinization may help to maintain rifting once it has localised, it does not aid the formation of microcontinents (Tetreault and Buiter, 2013).

3) Back-arc extension related to roll-back of a subducting slab may create the extensional stresses necessary for rifting fragments from a continent. Localisation of extension in the overriding plate is aided by subduction processes such as slab dehydration and mantle wedge hydration in combination with mantle corner flow, which cause weakening of the overriding plate. As an example, the Lord Howe Rise was rifted from Australia by late Cretaceous opening of the Tasman Sea above a retreating slab (Schellart et al., 2006; Sdrolias et al., 2003).

4) The misalignment of rift axes and their subsequent linkage may isolate microcontinents. The Danakil horst in the Afar region may be described as a nascent microcontinent. Recent independent movement of the Danakil block relative to Nubia, Arabia and Somalia suggests that the Red Sea and Aden rifts could link through Afar. The Red Sea would then be abandoned and the Danakil would become a microcontinent (Eagles et al., 2002). Gernigon et al. (2012) suggest that Jan Mayen may have been isolated by an

overlap of two active ridge systems: the Aegir Ridge on the east and the northward propagating Reykjanes Ridge that created the Kolbeinsey Ridge on the west side of Jan Mayen.
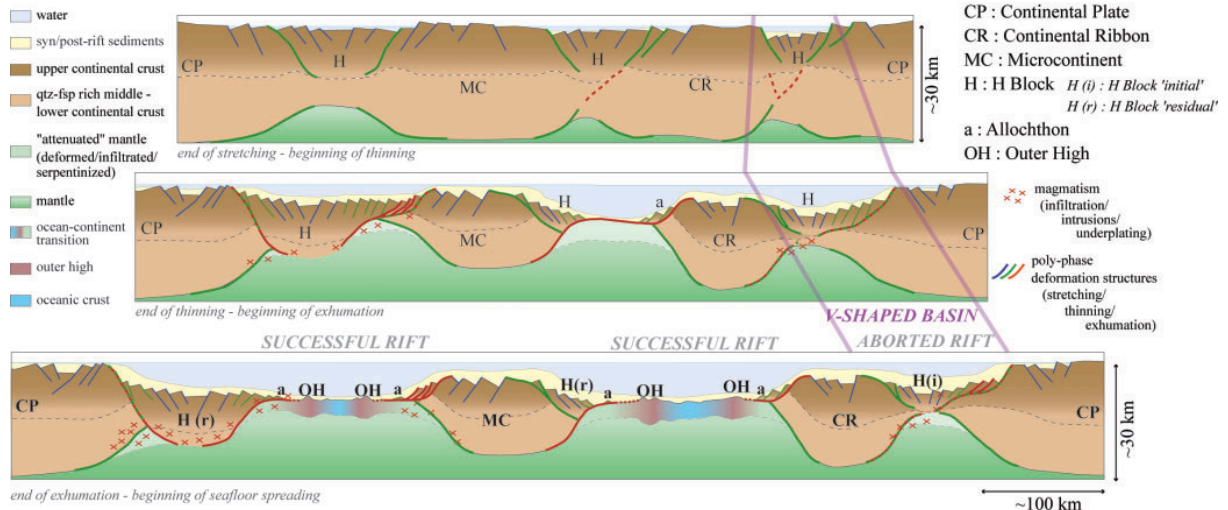

Figure 2: *Schematic evolution of a continental rift system from overall stretching (top), through localisation of deformation along a few faults in the thinning phase and the exhumation of mantle rocks (middle), to finally the isolation of continental ribbons (below). Figure from Péron-Pinvidic and Manatschal (2010).*
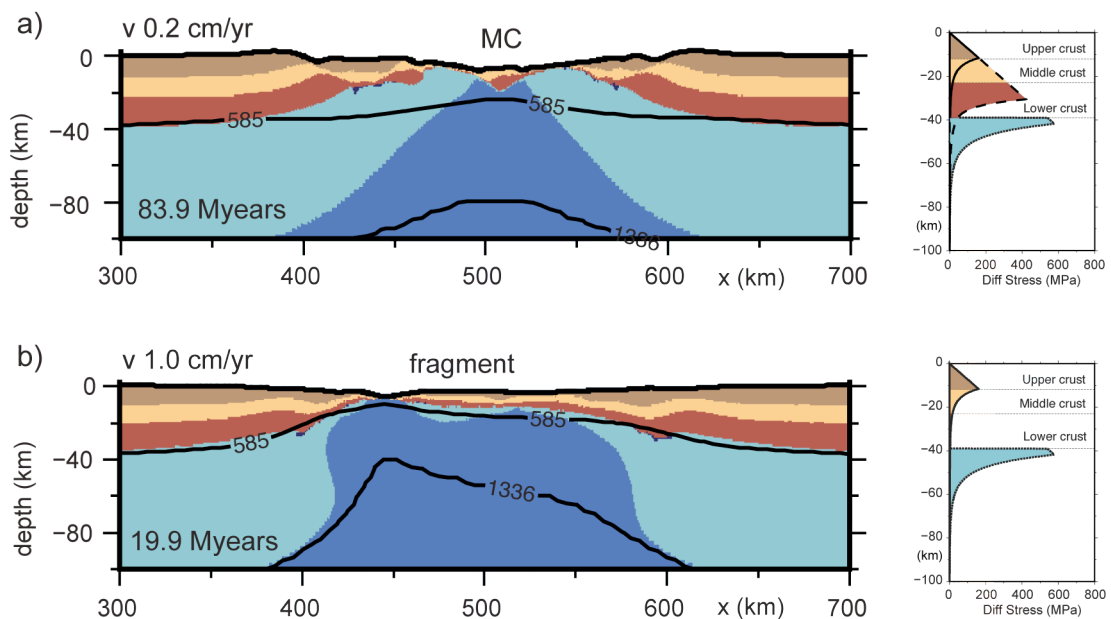

Figure 3: *Examples of 2-D dynamic models of the formation of continental fragments during different scenarios of passive margin formation. The results show a zoom of the 1000x410 km total model domain. The initial rheological layering is shown to the right. a) In a regime of ultraslow extension (overall extension velocity 0.2 cm yr^{-1}), two crustal regions are continuously thinned simultaneously, leaving a crustal block of mainly middle and lower crustal material. b) In this figure, continental fragments are created with moderate extension rates (1 cm yr^{-1}) and a spontaneous jump in rifting location. The deflection of the mantle upwelling, caused by the deflection of strain in the ductile lower crust, leads to an abandoned continental fragment. After Tetreault and Buiter (in prep.).*
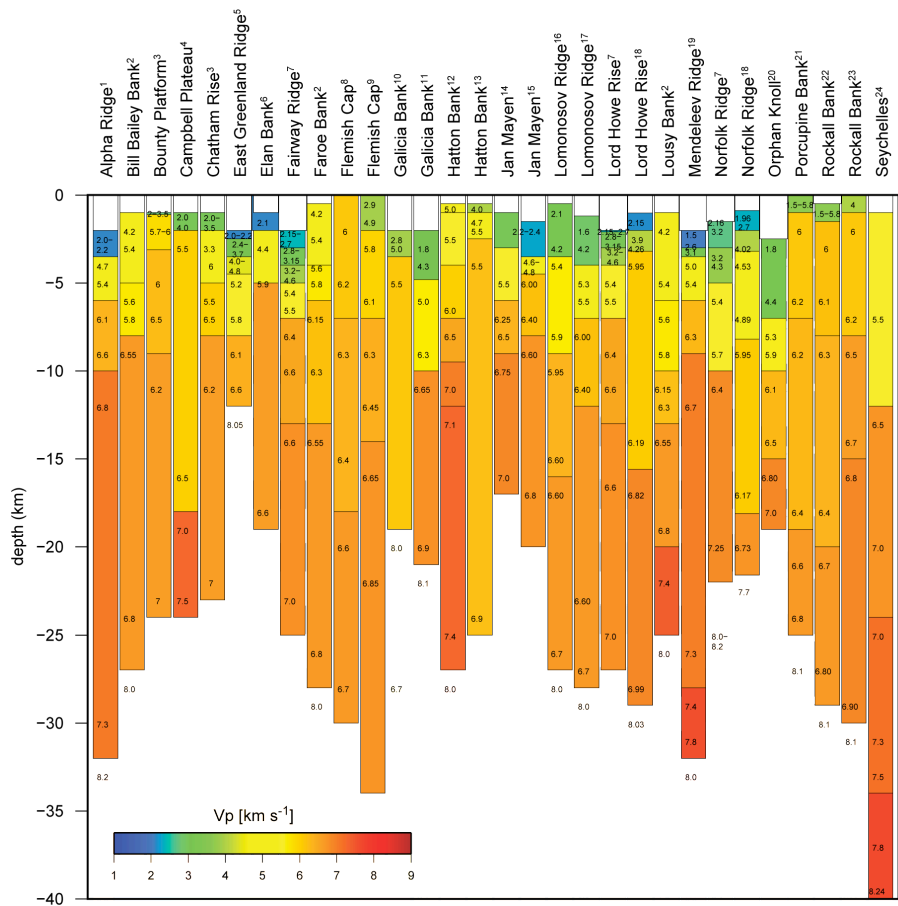
Figure 4: *Compilation of seismic velocity profiles of present-day microcontinents and continental fragments. From Tetreault and Buiter (2014, 2015).*

5) A lateral migration of the rift axis away from the continent, by multiple rift jumps, may isolate continental blocks. In multiphase rifting, phases of extension are separated by phases of tectonic quiescence during which conductive cooling may harden the initial rift site sufficiently to produce rift migration once extension resumes, thus isolating continental blocks (Braun, 1992; Naliboff and Buiter, 2015) (*Fig. 5*). This scenario always predicts different ages of rifting on each side of the continental fragment. The numerical experiments of Naliboff and Buiter (2015) indicate that tectonic quiet periods of over 20–60 Myrs between rifting stages are necessary to produce a jump in rift location.

6) Rifting may be guided away from locations of ongoing lithospheric thinning and jump towards a warm, weak region created by a mantle plume. Several microcontinents show close association with a hotspot, such as the Seychelles, Jan Mayen, and the Gilbert Seamount Complex (Müller et al. 2001, Gaina et al. 2003, 2009; Buiter and Torsvik, 2014). The close temporal relationships of break-up and flood basalt emplacement around the Seychelles microcontinent serve to illustrate that in many regions the debate regarding plume-assisted break-up versus magmatism caused by break-up is still very active (White and McKenzie, 1989; Todal and Eldholm, 1998; Collier et al., 2008). The Seychelles formed during break-up of Gondwana. In the Late Cretaceous, India and Seychelles rifted from Madagascar, opening the Mascarene Basin (Coffin and Rabinowitz, 1988; Müller et al., 1997). Spreading in the Mascerene Basin ceased progressively southward from ca. 67 to 59 Ma (Bernard and Munschy, 2000). Rifting on the east side of the Seychelles took place in stages. Rifting probably first occurred in the Gop Rift between India and the Laxmi Ridge, from ca. 71–66 Ma to ca. 56 Ma (Collier et al., 2008; Yatheesh et al., 2009). At this time, extension was therefore ongoing on both sides of the Seychelles. Break-up between the Laxmi Ridge and Seychelles at the

Carlsberg Ridge was younger, probably 63–62 Ma (Collier et al., 2008; Ganerød et al., 2011). This was shortly after the main eruption at 65 Ma of the Deccan large igneous province (Eldholm and Coffin, 2000; Courtillot and Renne, 2003), making it tempting to relate break-up to plume activity. In this plume-induced rift jump scenario, rifting may have been ongoing on both sides of the future microcontinent, with the plume teasing the active rift centre towards the other side, or rifting may be sequential through a rift jump.
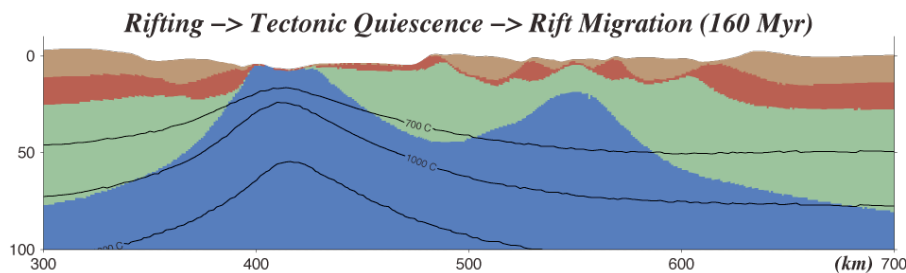

Figure 5*: Example of multiple stages of rifting separated by a tectonic quiet period in a numerical experiment (from Naliboff and Buiter, 2015). Zoom to the centre of a 1000 by 240 km finite-element model. Rifting begins with an overall extension velocity of 0.5 cm yr^{-1} during 85 Myr (creating the rift at x = 550 km), followed by 60 Myr cooling, and finally by a further 15 Myr of rifting. During the second rift phase, rifting jumps to the left ultimately leading to break-up there and creating a continental fragment.*

The above scenarios of the formation of microcontinents and continental fragments predict different ages of rifting on each side of a continental fragment (sequential and/or simultaneous rifting) and have different implications for the thermal environment in which rifting proceeds and sedimentary basins would form. Rifting in the presence of plumes or above a subduction zone would predict elevated crustal and lithospheric temperatures in comparison with rifting proceeding in magma-poor environments.

Previous numerical experiments show that the formation of microcontinents in a scenario of orthogonal (in 2-D experiments) passive margin evolution only occurs in special cases of ultraslow extension, or with a weak lower crust, or in systems where extension is interrupted by tectonic quiet phases (Tetreault and Buiter, in prep.; Naliboff and Buiter, 2015; *Figs. 3* and *5*). The few other numerical studies that have succeeded in creating a microcontinent have emplaced additional weak zones after rifting has begun. Yamasaki and Gernigon (2010) instantaneously emplaced a hot region (representing underplated mafic bodies) in the uppermost lithospheric mantle, without considering melting, and follow with emplacement of a similar hot region 100 km away after a certain amount of time has passed. Extension is initiated in the first emplaced hot body and may shift to the second body depending on the time offset, the lateral distance between the two bodies, and the temperature anomalies. While the numerical experiments do not create multiple extending regions in a dynamic manner and the ad-hoc emplacement of the mafic bodies controls the localisation of extension, it does confirm that extension only migrates in 2-D if the new future centre of extension is weak enough. Armitage et al. (2010) used finite-element models to examine rifting between India and the Seychelles in the Gop Rift and the Carlsberg Rift. Seafloor spreading in the Gop Rift is modelled as occurring above a hot mantle layer, which represents incubated Deccan (flood basalt) material that had spread laterally underneath the lithosphere. In the numerical experiment, the migration of extension from the Gop Rift to the Carlsberg Rift is imposed in order to estimate melt volumes, seismic velocity, and rare earth element chemistry of the melt.

So far only a very few geodynamic models of microcontinent formation in 2-D or 3-D exist and none have examined the influence of a rift jump towards a plume.

This report aims to apply scenarios of microcontinent formation to the Jan Mayen microcontinent. We first discuss the tectonic setting of Jan Mayen (*Chapter 2*), the timing of break-up, and scenarios for Jan Mayen formation from literature (*Chapter 3*). We then use dynamic numerical experiments computed with SULEC (*Chapter 4)* to test the following scenarios: 1) isolation of Jan Mayen that is initiated simultaneously on its western and eastern sides on inherited structures (in 2-D and 3-D, scenarios 1 and 4 above), and 2) isolation of Jan Mayen through a westwards rift jump towards the Iceland plume (in 2-D, scenario 6 above) (*Chapter 5*). The plume models include melt generation, migration and emplacement. These scenarios will clearly differ in terms of heat input into the system and the expected temperature evolution. We therefore specify surficial heatflow and the initial thermal structure of the models in addition to the evolution of lithology, topography, velocities, temperatures and viscosity.

2. THE TECTONIC SETTING OF JAN MAYEN

The Jan Mayen microcontinent lies in the North Atlantic Ocean between Norway and Greenland around latitude 70 ºN (Fig. 6). It is bound by the Kolbeinsey Ridge to the west, the extinct Aegir Ridge to the east, and the Jan Mayen Fracture zone and the Mohns Ridge to the north. Parts of proto-Jan Mayen were involved in the Caledonide collision (430–420 Ma) between Norway and Greenland. At that time, future Jan Mayen was located adjacent to what is now the Møre Margin of Norway and Jameson Land and the Blosseville Kyst of Greenland (Brekke et al., 2008). Break-up between Greenland and Jan Mayen on the one side and Norway on the other occurred ca. 55–53 Ma after a long period of several rifting phases that started in the Carboniferous (Talwani and Eldholm, 1977; Doré, 1991; Torsvik and Cocks, 2005). At this stage, the Mohns Ridge may have connected to the Aegir Ridge. The Aegir Ridge was abandoned at some time between 34 and 25 Ma (Gaina et al., 2009; Seton et al., 2012) and a ridge jump towards Greenland isolated Jan Mayen by ca. 23–20 Ma (Gaina et al., 2009; Gernigon et al., 2012). There is still uncertainty regarding the timings of rift initiation and cessation and this is discussed further in *Chapter 3*. After the ridge jump, the Mohns Ridge linked to the Kolbeinsey Ridge and Jan Mayen became part of Eurasia.
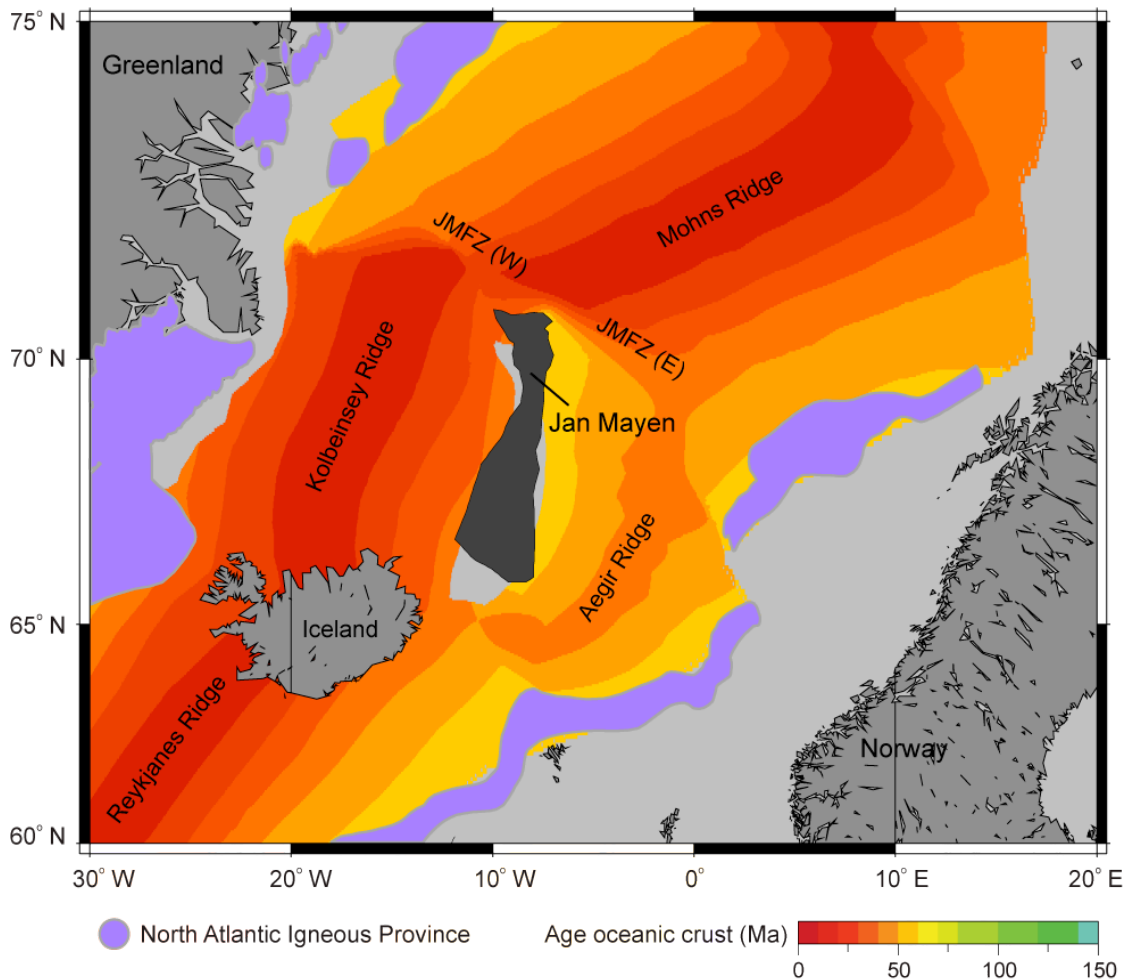

Figure 6*: The present-day setting of Jan Mayen with the North Atlantic Igneous Province (Coffin and Eldholm, 1992; Ganerød et al., 2010) superimposed on a map of oceanic crust ages (Müller et al. 2008). The general outline of continental crust under the Jan Mayen microcontinent is shown in dark grey and regions of voluminous magma are shown in purple. Light grey areas offshore have no identified magnetic anomalies and therefore no assigned age in Müller et al. (2008). JMFZ = Jan Mayen Fracture Zone.*

The Jan Mayen microcontinent is composed of a few continental blocks, including the main north-south trending Jan Mayen Ridge and the Southern Ridge Complex, and likely extends further south than shown in *Figure 6* (Foulger, 2006; Péron-Pinvidic et al., 2012a; Norwegian Petroleum Directorate, 2013; Torsvik et al., 2015). The Jan Mayen Trough separates the Southern Ridge Complex from the Jan Mayen Ridge. The present-day crustal thickness (not including sediments) of Jan Mayen varies from 7 to 24 km based on seismic refraction data (Kodaira et al., 1998; Kandilarov et al., 2012; see compilation in Tetreault and Buiter, 2015) and is thus substantially less than the crustal thickness of ca. 40 km onshore Norway (away from the margins) (Ottemöller and Midzi, 2003; Stratford et al., 2009).

The Jan Mayen Ridge is a narrow feature (<100 km wide) with an asymmetric crustal thickness (*Fig. 7*). To the west, the Jan Mayen Ridge gently thins into the Jan Mayen Basin, whereas to the east the continent-ocean transition abuts the ridge. The Jan Mayen Ridge and Southern Ridge Complex can be divided into two crustal layers. The upper crust has P-wave velocities ranging from 5.8–6.5 km s^{-1} and the lower crust has velocities of 6.7–7.0 km s^{-1} (Kodaira et al., 1998; Breivik et al., 2012; Kandilarov et al., 2012) (*Fig. 7*). The transition from continental crust to oceanic crust at the western margin of the Jan Mayen Ridge and the eastern margin of the Jan Mayen Basin is abrupt and based on interpreted oceanic affinity for crustal velocities. The lower crust in the ocean floor under the Norway Basin has values of 7.0–7.25 km s^{-1}, which are much greater than the typical continental values for that depth (Breivik et al., 2012). Seismic Profile 8-00 (*Fig. 7*) traverses the magmatic eastern margin of the Jan Mayen Ridge, but no magmatic underplating is convincingly identified (see also Kodaira et al., 1998). Breivik et al. (2012) suggest that the increase in seismic velocities in the lower crust to 7.0 km s^{-1} on the eastern margin of the Jan Mayen Ridge is evidence for magmatic underplating. However, these values are a bit low to be definitely considered magmatic, when compared to the velocities of typical underplated regions such as the Hatton Bank and Faroes (7.25–7.5 km s^{-1}). Nevertheless, the presence of some amount of basalt flow and intrusions in the sedimentary layers above the basement, in addition to seaward-dipping reflectors (SDRs) on the eastern margin of Jan Mayen, allow this margin to be characterized as 'magmatic'.

The continental flood basalts of the North Atlantic Igneous Province (NAIP) were emplaced in East and West Greenland, the Faeroe Islands and the British Isles (Saunders et al., 1997; Storey et al., 2007; Ganerød et al., 2010) (*Fig. 6*). The initial eruption at 63–61 Ma occurred before the plate separation of Europe and Greenland, but magmatism continued until after continental break-up. The average melt production rate increased by over an order of magnitude at 56 Ma, coinciding with continental break-up, and decreased drastically by 50 Ma (Storey et al., 2007). The NAIP flood basalts may link to the Iceland hotspot, but the validity of this link crucially depends on the location of the Iceland plume through time (Saunders et al., 1997; Storey et al., 2007; Meyer et al., 2007; Hansen et al., 2009; Ganerød et al., 2010). As discussed above, the eastern margin of Jan Mayen can be classified as magmatic based on SDRs, volcanic intrusions in sedimentary layers, and perhaps magmatic underplating (Skogseid and Eldholm, 1987; Mjelde et al., 2008; Breivik et al., 2012). In contrast, the western margin of Jan Mayen has been classified as non-volcanic (Gudlaugsson et al., 1988; Kodaira et al., 1998). However, sill-like intrusions occur in the sedimentary stratigraphy of possible late Oligocene–early Miocene age, which could be related to the break-up between Greenland and Jan Mayen (Gudlaugsson et al., 1988; Péron-Pinvidic et al., 2012a), and Mjelde et al. (2008) infer a thicker than average oceanic crust that they relate to increased magmatic influence of the Iceland plume.
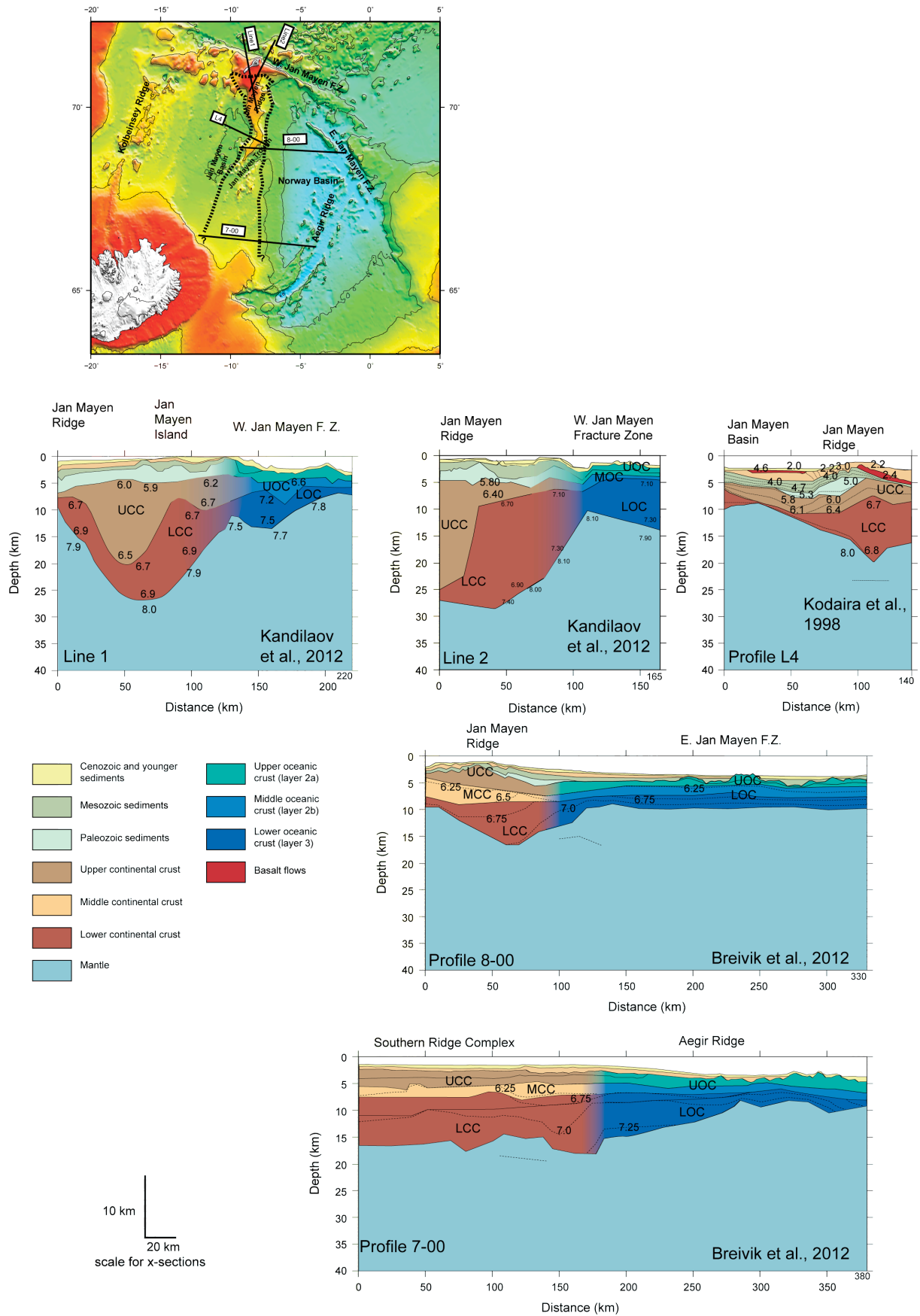
Figure *7: Location map of published seismic refraction lines that cross the Jan Mayen microcontinent. Lines modified from Kodaira et al. (1997), Breivik et al. (2012), and Kandilarov et al. (2012). Vertical exaggeration is 4:1.*

15

3. SCENARIOS FOR FORMATION OF THE JAN MAYEN MICROCONTINENT

The Jan Mayen microcontinent was isolated by abandonment of the Aegir Ridge on its eastern side and a ridge jump to the Kolbeinsey ridge on its western side. The crucial question regarding the formation of the microcontinent is: what could have caused the ridge jump? Once seafloor spreading was underway at the Aegir Ridge, oceanic mantle at this spreading centre would have been shallow, hot (>1300 ºC) compared to the surrounding cooled crust and thus weaker, making it very difficult to tease rifting away to a new rift centre within what was then possibly thinned continental crust of the Jan Mayen Basin between the Jan Mayen Ridge and Greenland. For any scenario of the formation of Jan Mayen, the time of cessation of seafloor spreading at the Aegir Ridge and the time of initiation of seafloor spreading at the Kolbeinsey Ridge is crucial because that determines whether both spreading centres were simultaneously active or whether there was a jump in time as well as location. In addition, though the time of emplacement of the NAIP flood basalts is well constrained, the position of their possible feeder plume, the Iceland plume, is less certain and depends on whether a fixed or moving mantle plume is assumed (Lawver and Müller, 1994; Mihalffy et al., 2008).

Stretching between Norway and Greenland occurred in several phases from the Carboniferous to the Paleogene, making it likely that extension also thinned the crust in the regions where the Aegir and Kolbeinsey Ridges later developed. The Jan Mayen microcontinent itself probably also experienced deformation related to late Cretaceous–Late Palaeocene rifting (Gaina et al., 2009). The first clearly identified magnetic anomaly between Jan Mayen (with Greenland) and Norway is anomaly 24 (Talwani and Eldholm, 1977; Nunns 1983), although older linear magnetic anomalies occur locally in the NE Norway Basin (Gaina et al., 2009). This places the initiation of seafloor spreading on the Aegir Ridge at ca. 55–53 Ma. Break-up regionally propagated from northeast to southwest in the Norway Basin (Gernigon et al., 2012; Péron-Pinvidic et al., 2012b). The Aegir Ridge seems to have failed to link to the active ridge in the northeast Atlantic Ocean to the south of Jan Mayen (the Reykjanes Ridge) (Gaina et al., 2009), but may have linked to the Mohns Ridge to the north. Problematic seafloor spreading in the Aegir Ridge caused Jan Mayen to rotate counter-clockwise and led to the development of fan-shaped magnetic anomalies in the Norway Basin (Talwani and Egholm, 1977; Gaina et al., 2009; Gernigon et al., 2012).

The time of cessation of seafloor spreading at the Aegir Ridge has been placed between ca. 25 Ma (anomaly C7) to 34 Ma (anomaly C13) (Talwani and Eldholm, 1977; Nunns, 1983; Jung and Vogt, 1997; Gaina et al., 2009; Gernigon et al., 2012). This range in interpreted ages likely occurs because magnetic anomalies between C12 (30.9–30.4 Ma) and C7 (24.8–24.7 Ma) are difficult to resolve due to the ultra-slow spreading character of the ridge during its last phases (Jung and Vogt, 1997). Because the final phases of spreading are very slow and disorganized, concurrent with the formation of several fracture zones, not much overall extension is recorded. We therefore follow the model of Gaina et al. (2009) and place the cessation of spreading at ca. 30 Ma.

The Aegir Ridge has a comparatively thin crust of 4–5 km thickness (Breivik et al., 2006), which could point to cool (normal) asthenospheric temperatures in the Oligocene (Greenhalgh and Kusznir, 2007). In the Miocene, asthenospheric temperatures likely were more elevated to produce the magmatic margin (Greenhalgh and Kusznir, 2007). Alternatively, Breivik et al. (2006) suggest the unusually thin oceanic crust of the Aegir Ridge is caused by northeast transport of depleted mantle from the magmatic Greenland-Iceland-Faeroe Ridge area to the Norway Basin.

Prior to break-up, stretching occurred between Jan Mayen and Greenland, possibly beginning around the Palaeozoic-Mesozoic (Kodaira et al. 1998; Gaina et al., 2009; Péron-Pinvidic et al., 2012b). Gaina et al. (2009) suggest that the Jan Mayen Basin (west of Jan Mayen) may have initiated in the Cretaceous and then later reactivated during final rifting leading to break-up between Jan Mayen and Greenland. The initiation of seafloor spreading on the Kolbeinsey Ridge has been placed at ca. 25–24 Ma (anomalies C7–C6c) (Talwani and Elhholm, 1977; Vogt et al., 1980), but the precise timing is unclear and could likely be older (Gaina et al., 2009; Péron-Pinvidic et al., 2012a; Gernigon et al., 2012). The Kolbeinsey ridge propagated from south to north. Gaina et al. (1990) suggest that the Kolbeinsey Ridge completely detached the southern part of Jan Mayen by C6 (20 Ma) and that a connection between the Kolbeinsey Ridge and the Mohns Ridge to the north was established via the Jan Mayen Fracture Zone by C5 (10.9 Ma). Gernigon et al. (2012) place complete break-up between Jan Mayen and Greenland slightly earlier at C6b (23–22.5 Ma).

The initial phase of seafloor spreading along the Kolbeinsey Ridge was associated with minor magmatism, but Mjelde et al. (2008) infer increased magmatic influence of the Iceland plume ca. 2 Myrs after break-up based on the thicker than average oceanic crust (*Fig. 8*). Kodeira et al. (1998) also suggest a slightly hotter than normal asthenosphere, possibly due to the influence of the Iceland plume. They explain the observation of only minor amounts of extrusive and intrusive volcanics by conductive heat loss because of the long duration of rifting.

We follow the kinematic evolution of the Jan Mayen microcontinent from the most recent reconstructions of Gaina et al. (2009), Gernigon et al. (2012), and Péron-Pinvidic et al. (2012b) (*Fig. 9*). *Figure 9* also shows the position of a stationary Iceland plume (fixed hotspot, Lawver and Müller, 1994) and the position of the Iceland plume if the effect of mantle convection is taken into account (moving hotspot, Mihalffy et al., 2008). The moving hotspot is closer to the future location of break-up than the fixed hotspot. However, even when plumes are offset from a rifting region, flow of warm plume material towards the rift (as an upside-down drainage flow, Sleep, 1997) could still weaken the rift area and thus help the lithosphere to achieve break-up (Buiter and Torsvik, 2014).

The cessation of seafloor spreading on the Aegir Ridge by ca. 30 Ma (or latest by ca. 25 Ma) and the initiation of seafloor spreading on the Kolbeinsey Ridge by ca. 25 Ma (or perhaps slightly older) implies that if seafloor spreading occurred simultaneous on both sides of Jan Mayen, it could not have been for very long. These timings effectively rule out a scenario of a rift jump caused by multiphase extension (scenario 5 in *Chapter 1*) because that microcontinent formation model would require over tens of Myr cooling time on the Aegir Ridge before a rift jump would occur to the Kolbeinsey Ridge (Naliboff and Buiter, 2015). Subduction in the region had ceased after Caledonide collision at ca. 430–420 Ma, ruling out microcontinent formation by slab roll-back (scenario 3). The scenarios of microcontinent formation (*Chapter 1*) that we can consider for Jan Mayen are therefore non-simultaneous localisation of extension in regions of pre-existing heterogeneity (scenario 1), a misalignment of rift axes (scenario 4), or a rift jump towards a mantle plume (scenario 6) (*Fig. 10*). We will test these scenarios in *Chapter 5*.
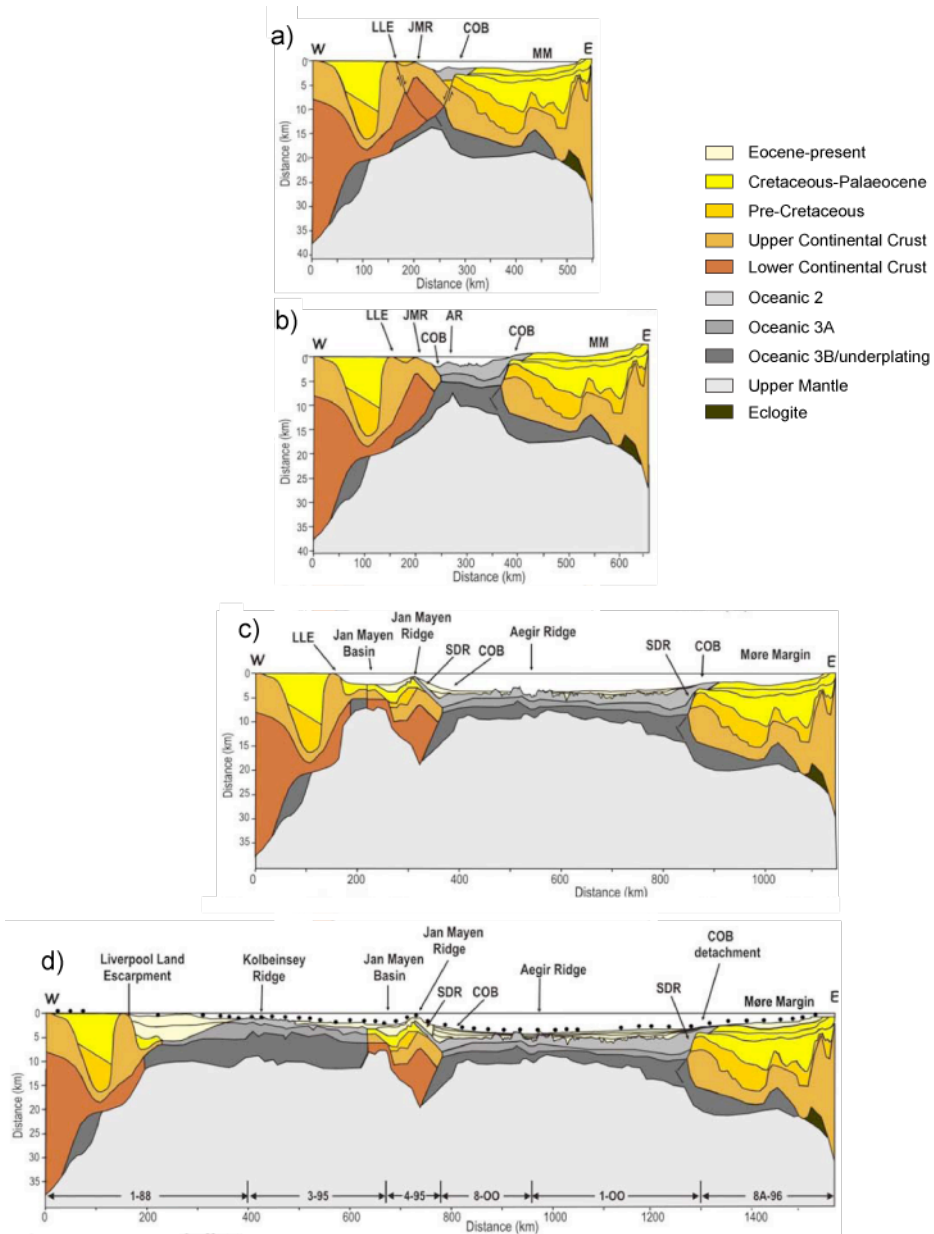
Figure 8: *Simple conjugate margin reconstruction from Mjelde et al. (2008) using crustal structure from seismic refraction analyses. a) Break-up at 55 Ma is suggested to have been slightly asymmetric. b) Seafloor spreading on the Aegir Ridge visualised at 52 Ma, c) Section at 25 Ma shows the Jan Mayen basin just before break-up. d) Smoothed and interpreted present-day transect based on ocean bottom seismograph surveys. AR = Aegir Ridge, COB = Continent-Ocean-Boundary detachment, JMR = proto Jan Mayen Ridge, LLE = Liverpool Land Escarpment (detachment), MM = Møre Margin, and SDR = Eocene Flood Basalt/Seaward Dipping Reflectors.*
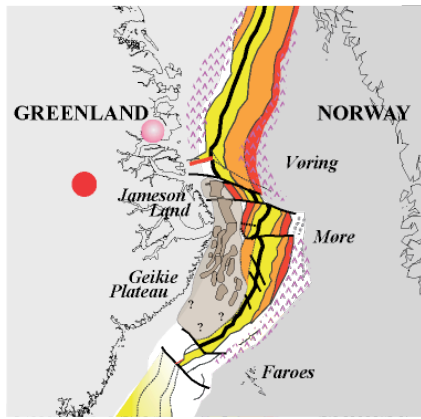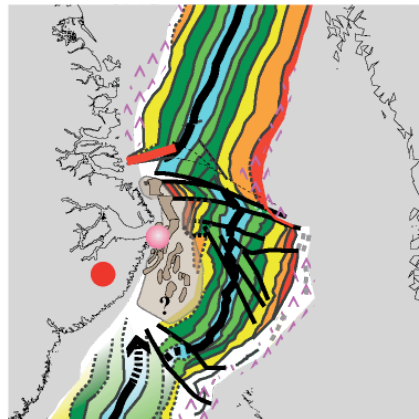
C22: Late Ypresian (49.7 Ma)
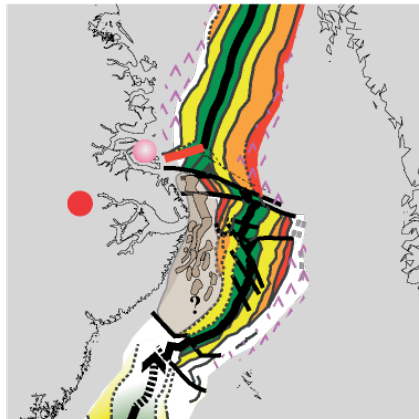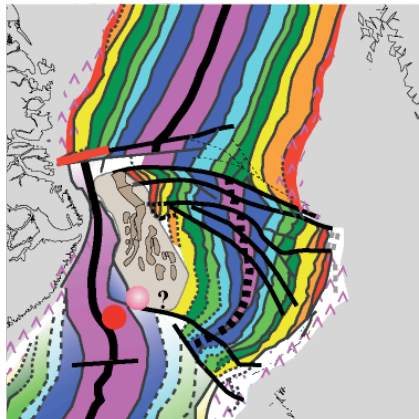
C21: Lutetian (47.9 Ma)
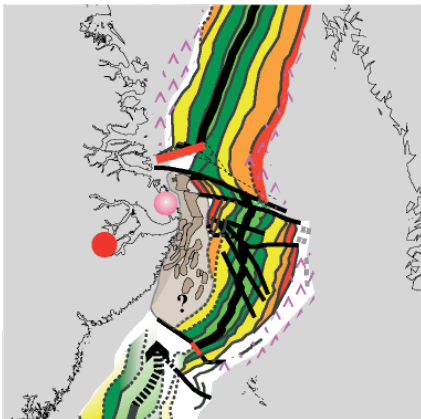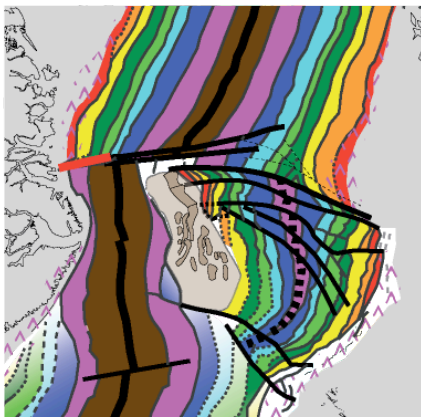
C20: Late Lutetian (43.8 Ma)

C18: Bartonian (40.1 Ma)

C13: Priabonian (33.1 Ma)

C6: Early Miocene (20.1 Ma)

C5: Mid. Miocene (10.9 Ma)

> chron C24b	> chron C20
> chron C24a	> chron C18
> chron C23	> chron C13
> chron C22	> chron C6
> chron C21	> chron C5

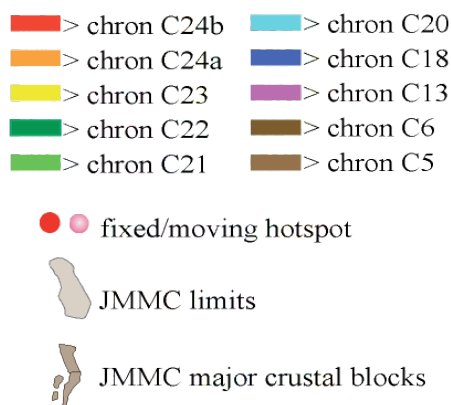● ○ fixed/moving hotspot

JMMC limits

JMMC major crustal blocks

Figure 9:
Kinematic evolution of the Jan Mayen microcontinent (JMMC). From Péron-Pinvidic et al. (2012b) (which was modified from Gaina et al. (2009) and Gernigon et al. (2012)). Fixed hotspot position from Lawver and Müller (1994), moving hotspot from Mihalffy et al. (2008).
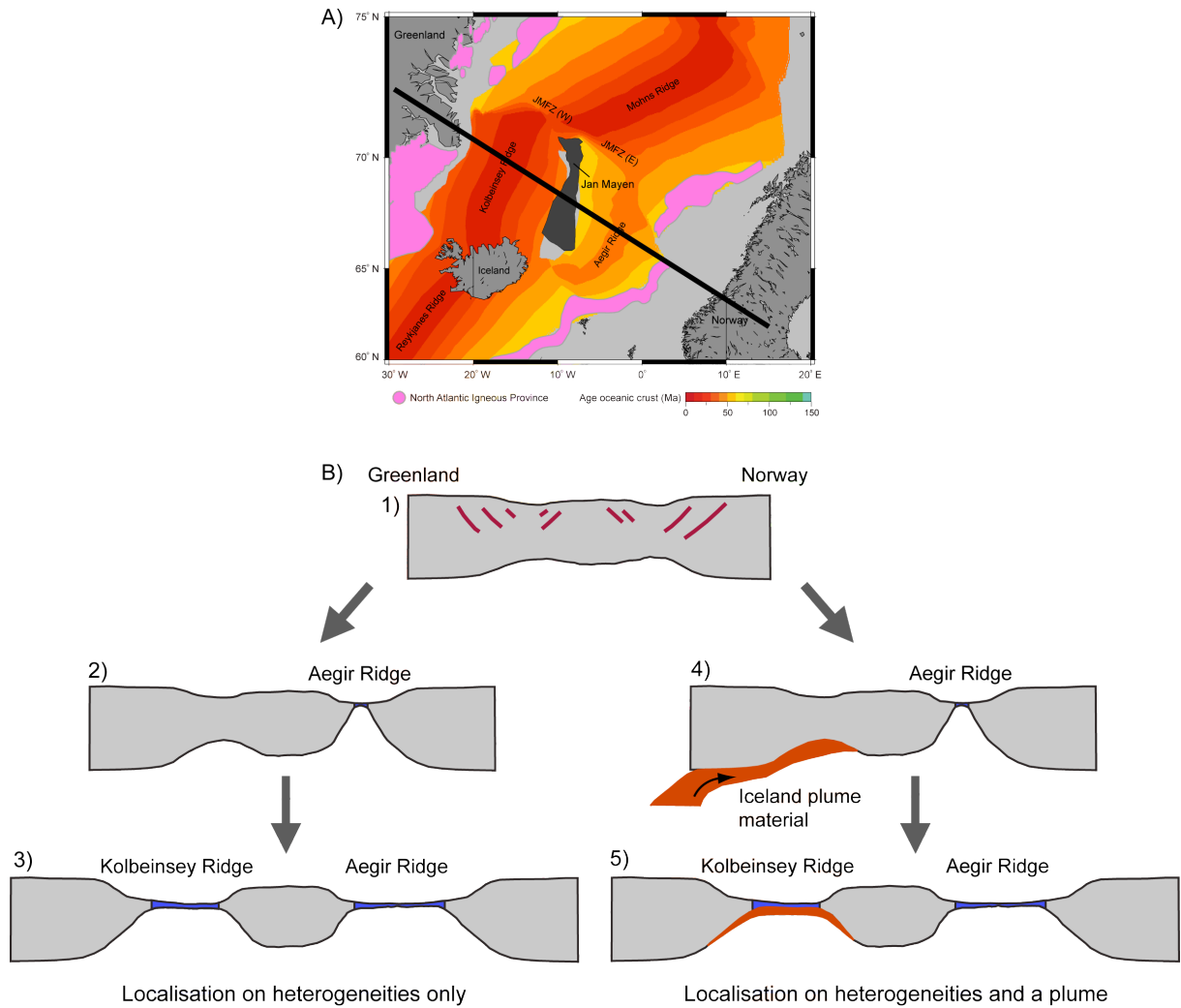
Figure 10: *Cartoons of Jan Mayen scenarios to test with numerical experiments in Chapter 5. A) Approximate location of section. B1) Norway-Greenland in the Cretaceous. B2 and B4) Reactivation of inherited structures leads first to break-up at the Aegir Ridge. B3) Subsequent reactivation of inherited structures or far-field forces lead to break-up at the Kolbeinsey Ridge. B5) Break-up at the Kolbeinsey Ridge is triggered by warm and weak material of the Iceland Plume arriving in the rift zone.*

4. NUMERICAL MODELLING APPROACH

4.1 Set of equations and modelling code SULEC

We will test scenarios for formation of the Jan Mayen microcontinent with numerical models. This Chapter describes the numerical background for these models. We solve the incompressible momentum equation for slow creeping flows:

$$\nabla \bullet \sigma' - \nabla P + \rho g = 0$$
$$\nabla \bullet u = 0$$

1

ρ is density, g gravitational acceleration (written as a vector with $g_x = 0$ and $g_y = 9.81$ m s^{-2}), and u velocity. The dynamic pressure P is computed using an iterative penalty (Uzawa) formulation (Cuvelier et al., 1986; Pelletier et al., 1989; Zienkiewicz and Taylor, 2000). We monitor the divergence of the velocity field ($\nabla \bullet u$) as a convergence criterion for the accuracy of the pressure field (Pelletier et al., 1989). The deviatoric stress tensor σ' relates to the deviatoric strain-rate tensor $\dot{\varepsilon}'$ following an effective viscosity η_{eff}:

$$\sigma' = 2\eta_{eff}\dot{\varepsilon}'$$
$$\dot{\varepsilon}'_{ij} = \frac{1}{2}\left(\frac{\partial u_i}{\partial x_j} + \frac{\partial u_j}{\partial x_i}\right)$$

2

The materials in our models behave either viscous or plastic (brittle). Plastic failure occurs when the deviatoric stress reaches the yield stress:

$$\sigma'_2 = P\sin\phi + C\cos\phi$$

3

ϕ is the angle of internal friction and C is cohesion. We use a linear softening of the angle of internal friction between ϕ_1 and ϕ_2 (*Table 1*) over an interval of finite strain of 0.5–1.5. This mimics softening of shear zones because of foliation development, mineral transformations, and grain size changes (Mandl, 1988; Rice, 1992; Bos and Spiers, 2002; Lacroix et al., 2015). The effective viscosity for plastic flow is:

$$\eta^p_{eff} = \frac{P\sin\phi + C\cos\phi}{2\dot{\varepsilon}'_2}$$

4

σ'_2 and $\dot{\varepsilon}'_2$ are the second invariants of the deviatoric stress tensor and strain-rate tensor, respectively $\left(\sigma'_2 = \left(\frac{1}{2}\sigma'_{ij}\sigma'_{ij}\right)^{1/2} and \ \dot{\varepsilon}'_2 = \left(\frac{1}{2}\dot{\varepsilon}'_{ij}\dot{\varepsilon}'_{ij}\right)^{1/2}\right)$. Temperature-dependent power-law flow follows:

$$\eta^v_{eff} = \frac{1}{2}A^{-1/n}C_{OH}^{-r/n}d^{p/n}\dot{\varepsilon}'_2{}^{1/n-1}e^{\frac{Q+PV}{nRT}}$$

5

A is the power-law exponent, n power, C_{OH} water content, r water exponent, d grain size, p grain size exponent, Q activation energy, V activation volume, R gas constant, and T temperature. For the sub-lithospheric mantle, the effective viscosity is a composite of dislocation and diffusion creep (van den Berg et al. 1993):

$$\eta = \left(\frac{1}{\eta_{disl}} + \frac{1}{\eta_{diff}} \right)^{-1} \qquad\qquad 6$$

We use flow laws for wet quartzite for the upper-middle crust, wet anorthite or gabbro for the lower crust, and dry olivine for the sub-crustal mantle (Hirth et al., 2001; Rybacki et al., 2006; Zhou et al., 2012; Hirth and Kohlstedt, 2003). For typical lithospheric viscosities of 10^{22}–10^{24} Pa s and a shear modulus of 5 x 10^{10} Pa, the Maxwell time is on the order of 6–600 kyr and the Deborah number $\ll 1$, indicating that elastic deformation is not expected to play a significant role (Reiner, 1964). We therefore ignore elastic deformation. The viscosity in the models is restricted to between 10^{18}–10^{26} Pa s. This is sufficient to capture the behaviour of a rifted margin system where viscosities are expected to vary over several orders of magnitude. Density is temperature-dependent following the Boussinesq approach:

$$\rho = \rho_0 \left(1 - \alpha \left(T - T_0 \right) \right) \qquad\qquad 7$$

ρ_0 is the density at temperature T_0 and α is thermal expansivity.

Because non-Newtonian (power-law) viscous flow and the Boussinesq density are dependent on temperature, we additionally solve the heat equation:

$$\rho c_p \left(\frac{\partial T}{\partial t} + u \bullet \nabla T \right) = k \nabla^2 T + H + 2 \sigma_2' \bullet \dot{\varepsilon}_2' \qquad\qquad 8$$

c_p is specific heat, k thermal conductivity, H heat production, and $2 \sigma_2' \bullet \dot{\varepsilon}_2'$ the shear heating term.

We discretize the model domain with quadrilateral elements with a continuous linear velocity field and constant, discontinuous pressures. Material properties are stored on tracers and advected at the end of each time step with a second-order Runge-Kutta advection scheme. To keep code memory requirements reasonable, tracer density is maintained between 8 and 18 per element, through tracer injection and deletion. We use harmonic averaging of tracers to elements for viscosity, and arithmetic averaging for density. The models have a true free surface that is achieved by column-wise slightly expanding or shrinking the Eulerian grid (Fullsack, 1995). We include a stabilisation term to stabilize numerical overshoot across density interfaces (Kaus et al., 2010; Quinquis et al., 2011). All material parameters used in our models are listed in *Table 1*.

We solve the set of equations using the Arbitrary Langrangian-Eulerian finite-element code SULEC-2D. SULEC uses the direct solver PARDISO (Schenk and Gärtner, 2004). SULEC has been used for modelling subduction, collision and terrane accretion (Quinquis et al., 2011; Tetreault and Buiter, 2012; Ghazian and Buiter, 2013, 2014; Quinquis and Buiter, 2014), extension and rifting (Ellis et al., 2011; Tetreault and Buiter, in prep.; Naliboff and Buiter, 2015) and has passed a wide range of analytical and community benchmark studies (e.g. Blankenbach et al., 1989; Crameri et al., 2012).

4.2 Modelling of melt generation, migration and emplacement

We calculate the generation and migration of melt in the mantle during extension based on the equations for decompression melting and two-phase flow. Melt generation is modelled by

calculating the degree of melting f using the peridotite parameterization of Katz et al. (2003). $f_{(T,P)}$ is the degree of melt that is possible to generate in the rock at temperature T and pressure P:

$$f_{(T,P)} = \frac{T - T_{sol}}{T_{liq} - T_{sol}}$$
$$T_{sol} = 1085.7°C + \left(132.9°C \cdot GPa^{-1}\right)P - \left(5.1°C \cdot GPa^{-2}\right)P^2 \qquad\qquad 9$$
$$T_{liq} = 1780°C + \left(45.0°C \cdot GPa^{-1}\right)P - \left(2.0°C \cdot GPa^{-2}\right)P^2$$

T_{sol} and T_{liq} are the temperature and pressure dependent solidus and liquidus curves for peridotite (Katz et al., 2003). The total depletion (D) that the rock has undergone is recorded because the melt will eventually be extracted and migrated away. The actual melt fraction M that is generated per time step is taken as the difference of the degree of melting from the total depletion:

$$M_t = f_{(T,P,t)} - \sum D \qquad\qquad 10$$

Once an element has reached a depletion ($\sum D$) equivalent to or greater than the possible melt fraction, $f_{(T,P)}$, no more melt can be generated.

The degree of depletion is advected along with the mantle material (the solid). But, the melt weight fraction, M, will vary locally due to extraction and migration (Schmeling, 2000). Following previous numerical studies (e.g. Ghods and Arkani-Hamed, 2000; Schmeling, 2010; Gerya, 2013), we only assume melt is extracted and mobile after 2% of melt is attained in a rock. However, unlike most numerical experiments of extension and decompression melting, we allow melt to percolate and migrate to the surface instead of removing the melt fraction and instantaneously placing it at the surface to create oceanic crust. By including melt migration, we can include the influence of melt transport and intrusion on the extensional regime within our numerical experiments. This migration step is consistent with geochemical studies of MORBs (mid-ocean ridge basalts) that find that the depletion and enrichment of certain elements do not match the source rock and must therefore have been supplied by melt originating elsewhere (*Fig. 11*) (Kelemen et al., 1997). Melt is believed to migrate through tubes in the solid mantle, and melt mobility is reliant on the amount of melt (Kelemen et al., 1997). We implement melt migration in our numerical experiments by calculating the velocity and displacement of melt based on the equations of two-phase flow. In two-phase flow, melt is migrated vertically in relation to the solid velocity, following Darcy's law (McKenzie, 1984; Spiegelman and McKenzie, 1987; Ghods and Arkani-Hamed, 2000). The melt velocity, v_m, is determined from the following relationship:

$$v_m = v_s - \frac{k_\varphi}{\varphi \mu_m}\left(\nabla P_m + \rho_m g \hat{z}\right) \qquad\qquad 11$$

v_s is the velocity of the matrix solid (mantle material), k_φ the permeability, φ the melt volume fraction or porosity, μ_m the melt viscosity, ρ_m the melt density, g gravity, $\hat{z}$ is the unit vector in the z-direction, and ∇P_m is the melt pressure gradient (McKenzie, 1984). The melt pressure gradient is due to matrix shear and compaction and is considered negligible when compared to the buoyancy factor (Scott and Stevenson, 1989; Mittelstaedt et al., 2011), and is therefore neglected in our calculations. We use a value of 10 Pa s for the melt viscosity, μ_m, which is within the range of 1 to 100 Pa s for basaltic to andesitic melt (Turcotte and Morgan, 1992).

We give the melt density, ρ_m, a constant value of 2800 kg m^{-3}, following Spiegelman and McKenzie (1987) and Ghods and Arkani-Hamed (2000).
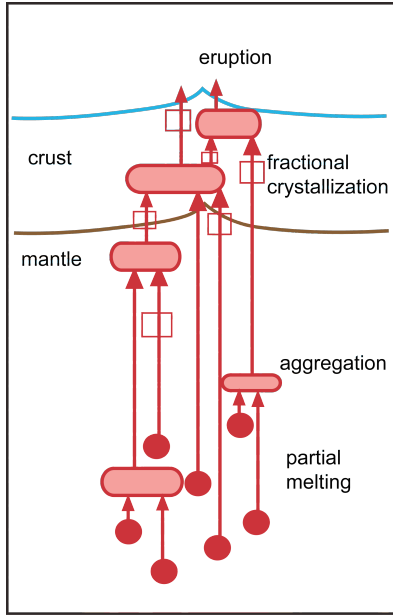

Figure 11: Schematic drawing of melt generation, migration, and crystallization. Modified from Grove et al. (1992).

Because we do not use a true two-phase flow system, we do not calculate the evolution of porosity and compaction. Instead, we take porosity to be equal to the melt volume fraction X, defined by McKenzie (1984) for a system with constant entropy, to be related to the melt weight fraction M. In our experiments we calculate the volume fraction relative to the depletion, which is the total weight fraction of melt produced by the rock:

$$\varphi = X = \frac{D\rho_s}{\rho_m + D(\rho_s - \rho_m)} \qquad\qquad 12$$

ρ_m and ρ_s are the density of the melt and the solid, respectively. Permeability, k_φ, is given by the following relationship:

$$k_\varphi = \frac{d^2\varphi^k}{c} \qquad\qquad 13$$

The constant d represents grain size (1 mm in our experiments) and c is a permeability constant of 1000 (Spiegelman and McKenzie, 1987; Ghods and Arkani-Hamed, 2000). The grain size of upper mantle material ranges from 1 cm (Ghods and Arkani-Hamed, 2000) to 1 mm (Spiegelman and McKenzie, 1987; Turcotte and Morgan, 1992). Larger grain sizes will lead to larger permeability values, and faster fluid velocities. The exponent k represents the relative connectivity of the porous media. A value of 2 for k represents a permeability system of fully connected tubes, while 3 is related to diffuse heterogeneous and less connected systems (Zhu and Hirth, 2003).

Melt migration is rapid enough (1–50 m yr^{-1}: Kelemen et al., 1997) that heat is not lost during transport (Furlong and Fountain, 1986). After melt is moved upwards, we change the temperature of the region of emplaced melt to represent the heating due to melt injection:

$$T = T_o + (T_m - T_o)\left(\frac{M}{M_{max}}\right)$$ 14

M_{max} is the maximum amount of melt that forsterite can hold. It is set to 0.20 in our models, which is the value at which clinopyroxene (cpx) is melted completely, leaving a fully depleted olivine (Asimow et al., 2004). T and T_0 are the temperatures at the region of emplacement after and before melt injection, T_m is the temperature of the melt at the source (we use the mantle potential temperature of 1300 ºC in our experiments).

The density of mantle material is affected by depletion and enrichment, and is perhaps the primary mechanical parameter affecting crustal deformation by intruding melt (Kohlstedt and Holtzmann, 2009). We factor in these effects by adjusting the Boussinesq density equation (*eq. 7*):

$$\rho = \rho_o\left(1 - \alpha(T - T_o)\right) + \varphi\Delta\rho_{depl} + M\Delta\rho_{en}$$ 15

α is heat expansivity, ρ_0 is the density at $T = T_0$, $\Delta\rho_{depl}$ is the change in density of depletion, $\Delta\rho_{en}$ is the change in density due to melt enrichment, and M is the total amount of melt (including melt migrated in from elsewhere) in that element. $\Delta\rho_{depl}$ and $\Delta\rho_{en}$ have values of -72.6 kg m^{-3} and -500 kg m^{-3} (Schutt and Lesher, 2006).

Laboratory experiments on mantle rocks with partial melt have demonstrated the weakening effect that melt has on olivine and peridotite rich rocks (Mei et al., 2002). Therefore we adjust the viscosity according to the flow law for upper mantle materials (*eq. 5*) with partial melt as defined by Mei et al. (2002):

$$\eta_{eff}^v = \tfrac{1}{2} A^{-1/n} C_{OH}^{-r/n} d^{p/n} \dot{\varepsilon}_2'^{1/n - 1} e^{\frac{-\beta M}{n}} e^{\frac{Q+PV}{nRT}}$$ 16

Here $\dot{\varepsilon}_2'$ is the second invariant of the strain rate tensor, σ'_2 the second invariant of the differential stress tensor, A the power law pre-exponent, C_{OH} water content, r the water content exponent, d grain size, p the grain-size exponent, n the power law index, Q activation energy, V activation volume, and R the gas constant. The creep dependence on melt fraction is given by the factor $exp(-\beta M/n)$, where β is found to be around 28 based on laboratory experiments of basalt with partial melt (Mei et al., 2002). The high percentage of melt fraction, in combination with the hot temperatures, significantly lowers the viscosities of the mantle in the region of the magma chamber.

4.3 Model setup

The model continent is composed of three crustal layers with 12, 11, and 16 km thicknesses and an 83-km thick lithospheric mantle that is underlain by upper mantle down to 410 km depth (*Fig. 12*). The 2-D model domain is divided into 700 by 160 finite-element cells, which have highest resolution in the future rift region (0.5 km wide by 1 km high over the crust in the centre of the model decreasing to 4 by 4 km in the mantle at the bottom corners). The initial thermal field has a surface temperature of 0 °C, a Moho temperature of 585 °C and a base of the lithosphere temperature of 1337 °C fitting a geotherm for a 120 km-thick continental lithosphere (Hasterok and Chapman, 2011). The lithosphere is extended with an overall velocity of 1.0 cm yr^{-1}. The outward material flow is compensated by an inflow below the lithosphere. One or two weak seeds are placed just below the crust in the centre of the

model domain to ensure rift initiation at a location away from the model boundaries. The weak seeds have brittle strain-softened properties lower than the crust and mantle. The models are run until crustal and lithospheric break-up using Courant time steps between 200 and 20,000 yrs. Plume models have a plume initial excess temperature of 200 °C.
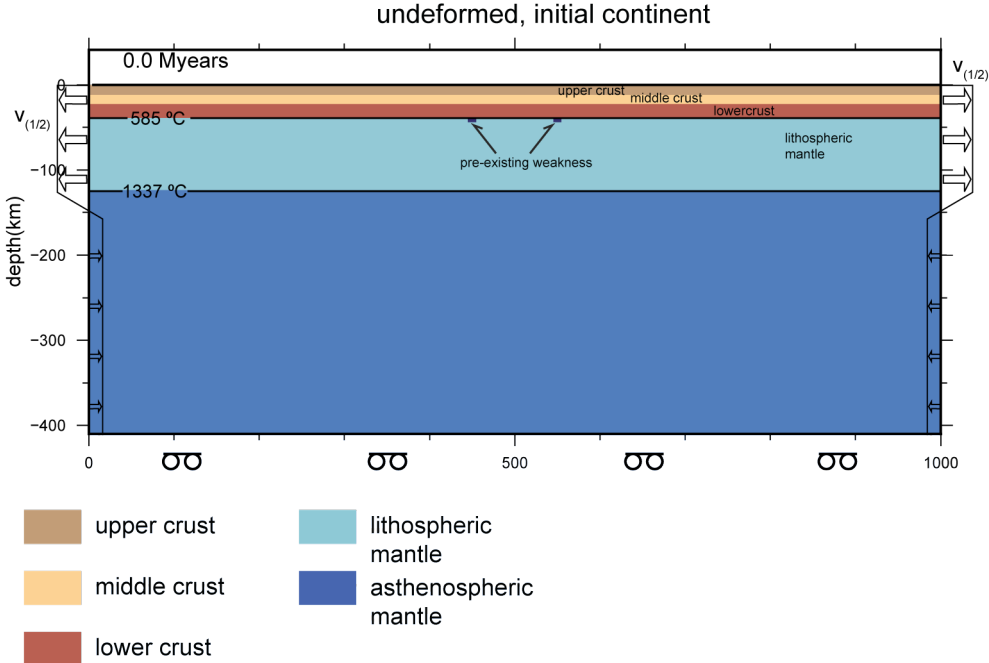

Figure 12: *Initial numerical model setup for extension of a continent initiated at two inherited weak regions.*

Table 1: *Material properties*

Parameter	Symb	Unit	Upper crust[a]	Middle crust[a]	Lower crust[b,c]	Mantle[d]
Reference density	ρ_0	kg m^{-3}	2600	2820	2900	3370
Reference temperature	T_0	ºC	0	0	0	600
Thermal expansivity	α	K^{-1}	-	-	-	2.5x10^{-5}
Heat capacity	C_p	J kg^{-1} K^{-1}	800	800	800	1000
Thermal conductivity	k	W m^{-1} K^{-1}	2.7069	2.4267	2.2060	82.9–3.0151[e]
Heat production	H	10^{-6} W m^{-3}	8.125x10^{-7}	4x10^{-7}	4x10^{-7}	2x10^{-8}
Angle of internal friction	ϕ_1, ϕ_2		20º – 10º	20º – 10º	20º – 10º	20º – 10º
Strain softening interval	ε_e		0.5 – 1.5	0.5 – 1.5	0.5 – 1.5	0.5 – 1.5
Cohesion	C	MPa	20	20	20	20
Flow law pre-factor[f]	A	Pa^{-n} m^p s^{-1} (H10^{-6}Si^{-1})$^{-r}$	6.31x10^{-36}	6.31x10^{-36}	Gabbro= 2.0x10^{-14}, Anorth= 1.58x10^{-18}	Diffusion= 1.58x10^{-15}, Dislocation= 1.58x10^{-21}
Flow law exponent	n		4.0	4.0	Gabbro= 4.0, Anorth= 3.0	Diffusion = 1.0, Dislocation= 3.5
Activation energy	Q	kJ mol^{-1}	135	135	644, 345	530, 375
Activation volume	V	10^{-6} m^3 mol^{-1}	0	0	0, 36x10^{-6}	18x10^{-6}, 1010^{-6}

Flow laws from: [a]Hirth et al. (2001); [b]Zhou et al. (2012); [c]Rybacki et al. (2006); [d]Hirth and Kohlstedt (2003). [e]Mantle conductivity is 82.9 W m^{-1} K^{-1} for T ≥ 1337 ºC and 3.0151 W m^{-1} K^{-1} for T < 1337 ºC for the models in Figs. 13, 20 and 21. The high value maintains the mantle adiabat in our models, which do not have vigorous mantle convection. The models in Figs. 19, 23 and 24 have a mantle conductivity of 3.0151 W m^{-1} K^{-1}; [f]A is converted to a general state of stress following Ranalli (1987).

5. EXPERIMENTS OF MICROCONTINENT FORMATION

5.1 Continental extension with inherited structures

Our first model has two seeds just below the Moho that represent in an extremely simplified manner deformational structures caused by stretching of the Norway-Greenland margins since the Carboniferous (scenario 1 in *Chapter 1*). We imagine that we pick up Jan Mayen evolution about late Cretaceous times. Initial stretching and rifting localises at each of the seeds, causing simultaneous crustal thinning until ca. 9 Myr model time (*Fig. 13*). With time, rifting localises in one of the basins, ultimately causing break-up there, while the other rift is abandoned. Once rifting shifts to one of the weak regions, the pattern is set and a microcontinent will not be created. This type of evolution over inherited structures in 2-D models is independent of rheological structure. We find from further tests (not shown here) that variations in crustal strength will change the amount of thinning on the abandoned rift. But once one of the rifts takes over and becomes the rheologically weaker area (*Fig. 13c*), the other is immediately abandoned in favour of deformation concentrating in the active rift.

This type of model could be seen as representing the initial phase of Jan Mayen development, with rifting occurring on each side of the microcontinent in the late stages of the Aegir Ridge and the early stages of the Kolbeinsey Ridge. The model clearly shows that inherited weak regions alone cannot produce two mid-ocean ridges and that therefore another factor or process is required to produce a microcontinent.
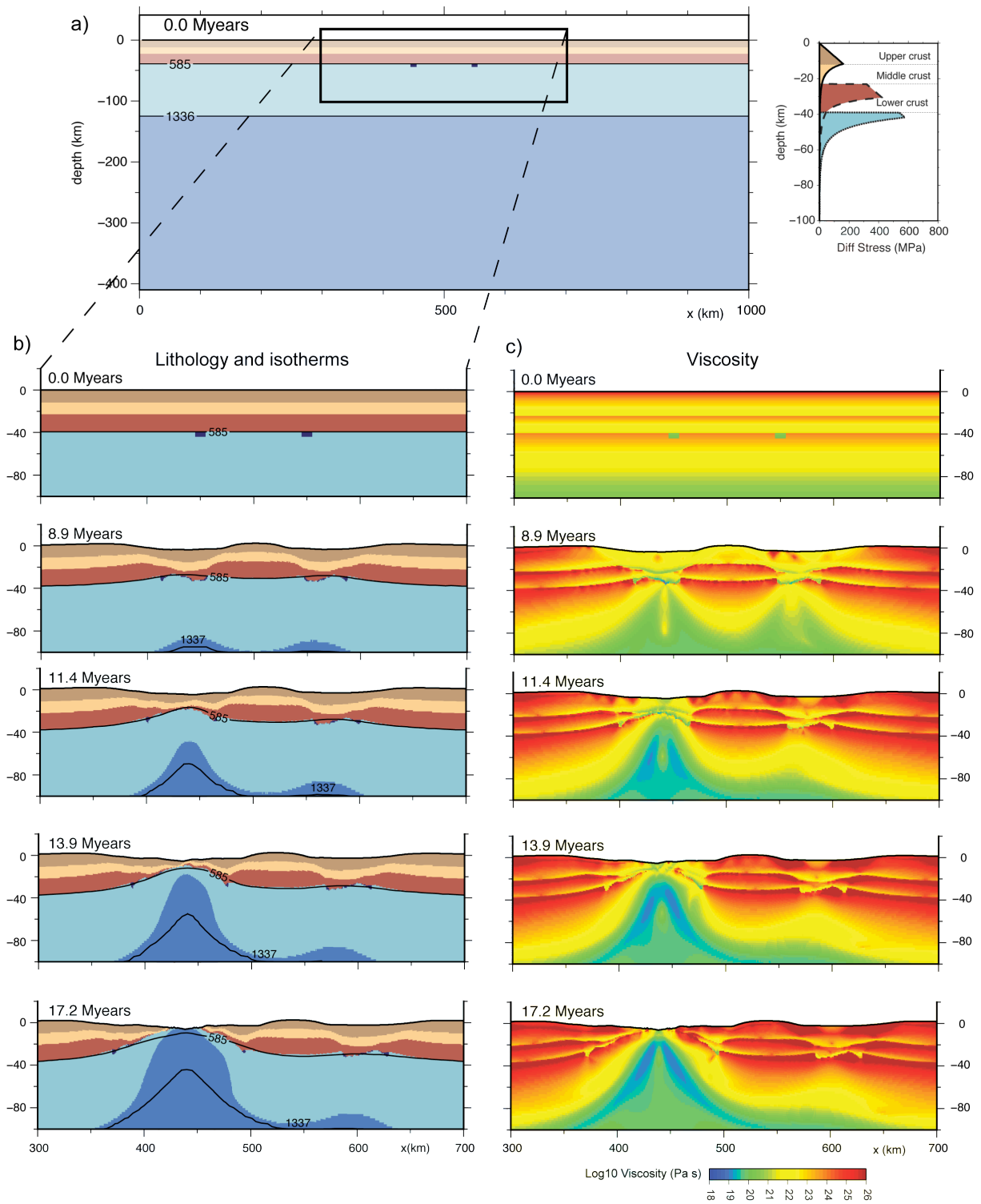
Figure 13*: Continental extension initiated on two inherited weak regions placed just below the Moho at 100 km horizontal offset. Extension initially occurs above each weak seed, until one region is abandoned and continental break-up occurs in one rift only. a) Setup of the model. This model follows rheological setup 2 of Tetreault and Buiter (in prep.) with a wet anorthite lower crust (Rybacki et al., 2006). b) Evolution of lithologies. The black lines are isotherms with temperatures in °C. c) Evolution of the viscosity field.*

5.2 Preliminary 3-D models of crustal-scale continental extension with inherited structures

It has been suggested that linking of rifts in 3-D may isolate microcontinents (scenario 4 in *Chapter 1*). We have run simple 3-D models to test whether linkage of weak structures in 3-D might create circumstances favourable for microcontinent formation. We first test crustal-scale models in which we can achieve a resolution that is high enough to well resolve brittle shear zones (*Figs. 14, 16*). These crustal-scale models are 360 km by 600 km by 20 (or 40) km (width x length x depth) with a resolution of 3 km in each horizontal direction, 1.25 km vertically in the upper crust and 2.5 km vertically in the lower crust. The upper crust is a brittle material, whereas the lower crust in the second model (*Fig. 16*) is a weak linear viscous material that is essentially providing an isostatic basal boundary to the upper crust. We introduce three weak regions offset from each other that represent locations where the Aegir Ridge, the Reykjanes Ridge and the Mohns Ridge would form. Our aim with the 3-D models is to test whether the weak regions on the left (the model Reykjanes and Mohns Ridges) would link up and create a structure resembling the Kolbeinsey Ridge and whether a transfer zone resembling the Jan Mayen Fracture Zone would form.
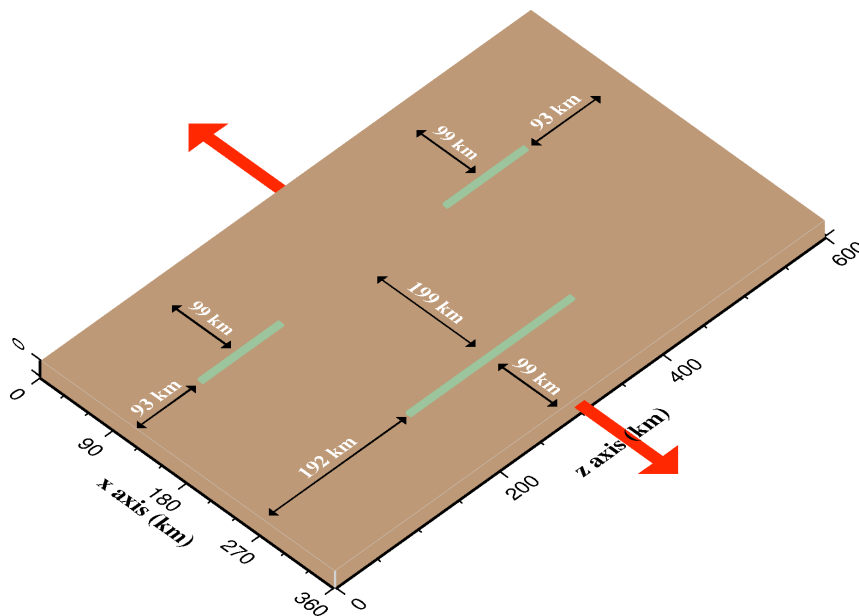

Figure 14: *Numerical setup for extension in the upper crust. The total horizontal extension rate, indicated by red arrows, is fixed at 1 cm/yr. Inflow at the base of the model prevents bulk thinning of the crust. A free surface at the top of the model allows topography to develop. The upper crust is 20 km thick and spans 360 km and 600 km, respectively, in the horizontal (x) and longitudinal (z) directions. Brittle deformation initiates along 'weak seeds' (in green) with a reduced angle of internal friction. The placement of the weak seeds reflects locations of the Aegir Ridge, the Reykjanes Ridge and the Mohns Ridge in a very schematic manner.*
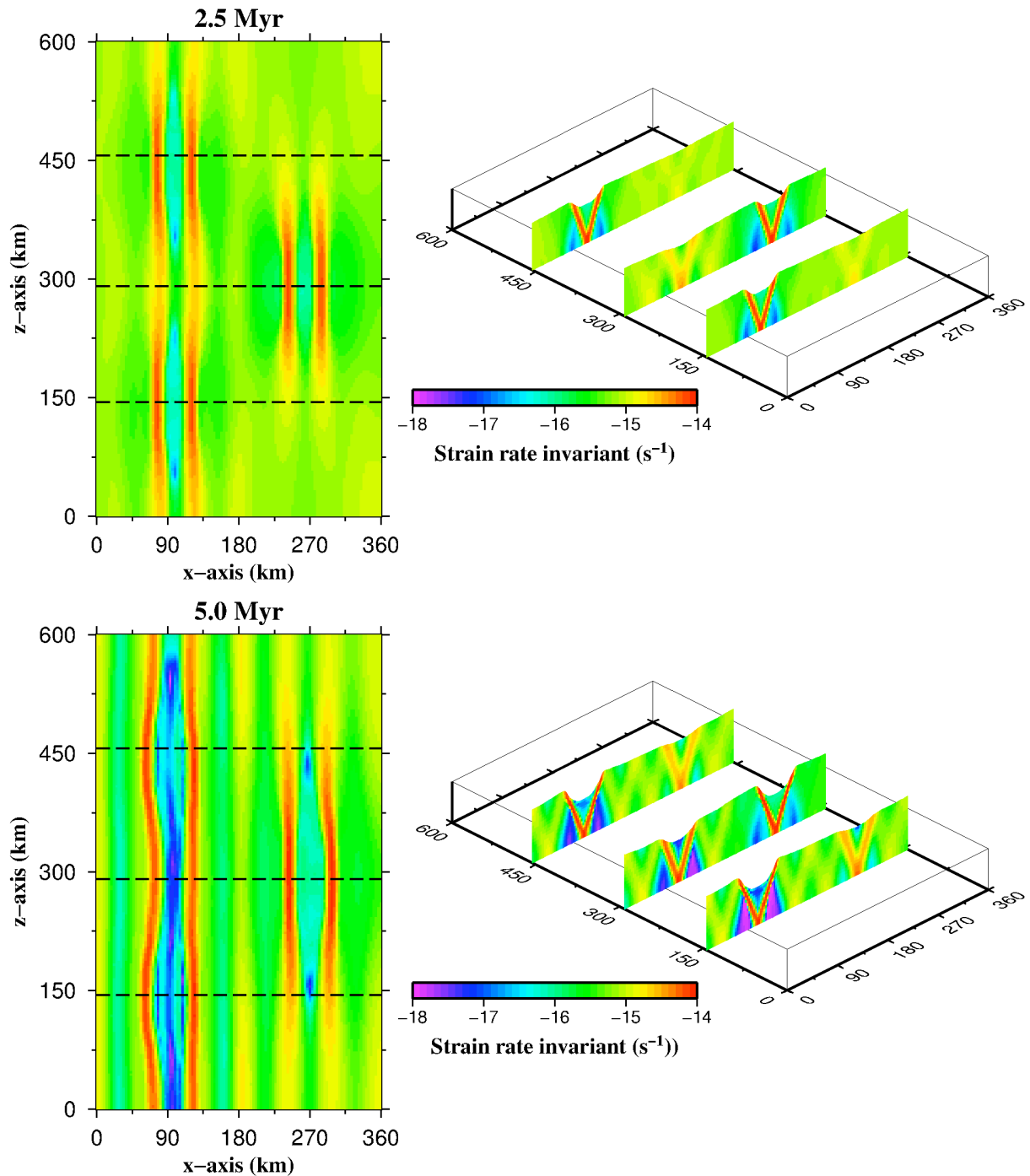
Figure 15: *Numerical results for extension in the upper crust after 2.5 Myr (Top) and 5.0 Myr (Bottom) for the setup in Figure 14. Left: Strain rate invariant at the model surface. Bands of high strain rate mark the surface expression of shear zones. Dashed lines parallel to the x-axis mark the location of vertical cross-sections of the strain rate invariant (Right). The vertical axis in the 3-D plots (Right) is exaggerated by a factor of 3. Through time, shear zones above the weak seeds propagate longitudinally, but transfer zones fail to develop between horizontally offset week seeds. This model made for this report by J. Naliboff, S. Buiter and J. Tetreault.*

Figures 15 and 17 show that extension in the crustal-scale models localises above the weak seeds, creating surface basins. In the upper crust model (*Figs. 14, 15*) rift propagation is limited and extension in the future Kolbeinsey Ridge region remains minor. No strike-slip zone that would be the equivalent of the Jan Mayen Fracture Zone forms, but instead the model tends towards the formation of two parallel ridges. Introduction of a lower crust leads to abandonment of the segments that represent the Reykjanes and Mohns Ridges and instead rifting propagates north and south from the weak zone that represents the Aegir Ridge (*Figs. 16, 17*).
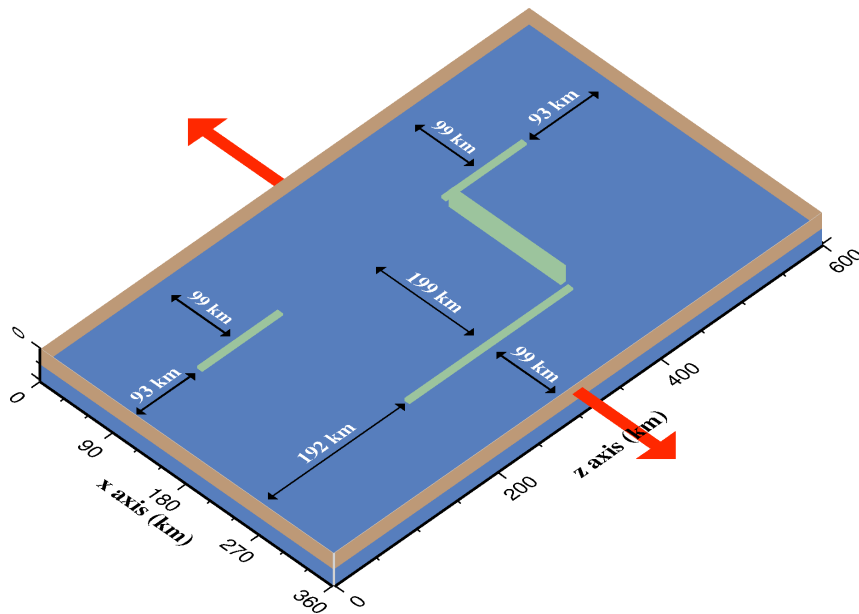

Figure 16: *Numerical setup for extension in the upper and lower crust. The numerical model is identical to Figures 14 and 15, with the exception of the addition of a weak lower crust (1e19 Pa s) and the addition of a 4th seed connecting two horizontally offset weak seeds. This connecting seed was added to see if a fracture zone (analogous to the Jan Mayen fracture zone) would initiate.*
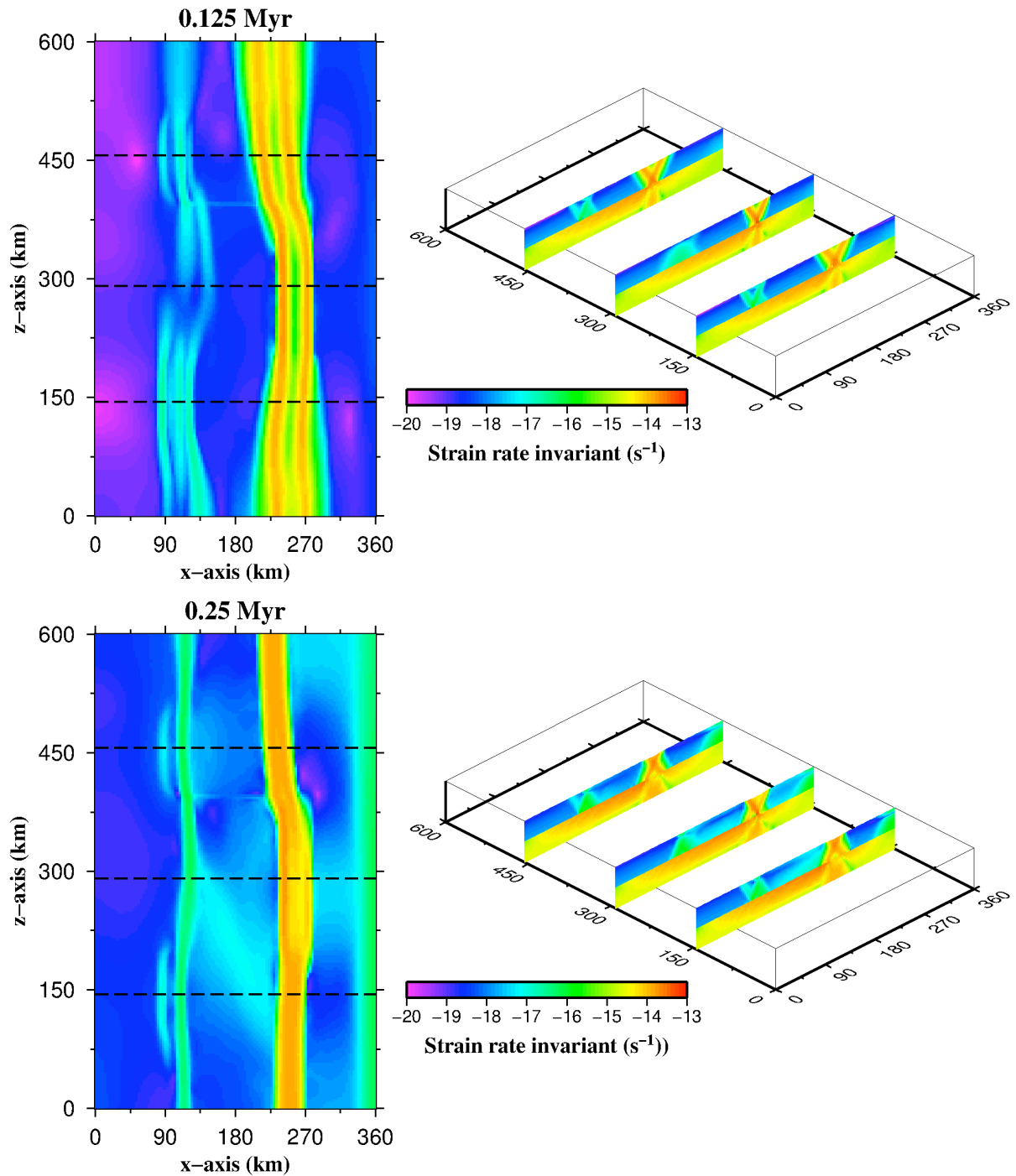
Figure 17: *Numerical results for extension in the upper and lower crust after 0.125 Myr (Top) and 0.25 Myr (Bottom) for the setup in Figure 16. The vertical axis in the 3-D plots (Right) is exaggerated by a factor of 1.5. In comparison to models without a lower crust, deformation rapidly focuses on the far right weak seed, while shear zones along the left side of the model are abandoned. This model made for this report by J. Naliboff, S. Buiter and J. Tetreault.*

We next test whether the introduction of a lithospheric mantle to 200 km depth and temperature-dependent viscous behaviour might modify our findings (*Figs. 18, 19*). The models are 480 km by 480 km by 200 km (width x length x depth). The increased depth of the model domain and the non-linear deformation behaviour introduced by the viscous creep law necessitate a lower grid resolution of 4–10 km (in each direction) in comparison with the crustal-scale models. In this experiment, we have three seeds parallel to the z-axis representing inherited weaknesses that are aimed at eventually becoming the Mohns, Kolbeinsey, and Aegir ridges. Two seeds, which have a higher viscosity than the ridge seeds, connect the offset Aegir seed on the right to the Mohns and Kolbeinsey seeds on the left (*Fig. 18*). These two seeds represent transfer faults. Due to their higher viscosity than the other three seeds, they will have a decreased ability to localise deformation. By having increased viscosity on the seeds representing the transfer faults, we hope to allow deformation to propagate between the two aligned seeds in the left representing the Mohns and Kolbeinsey ridges.

Figure 19 show how deformation localises above the weak regions. Despite having "stronger" seeds between the ridges, strain does not propagate between the two seeds on the left side of the model that represent the Mohns and Kolbeinsey ridges. Because the transfer zones are established and deformation is allowed to localise in these strike-slip shear zones, the two rifts do not propagate and join together.

These 3-D models confirm our findings from the 2-D models that inherited structure alone is not likely to induce a rift jump, isolating a microcontinent, again pointing to the need of an additional factor or process.
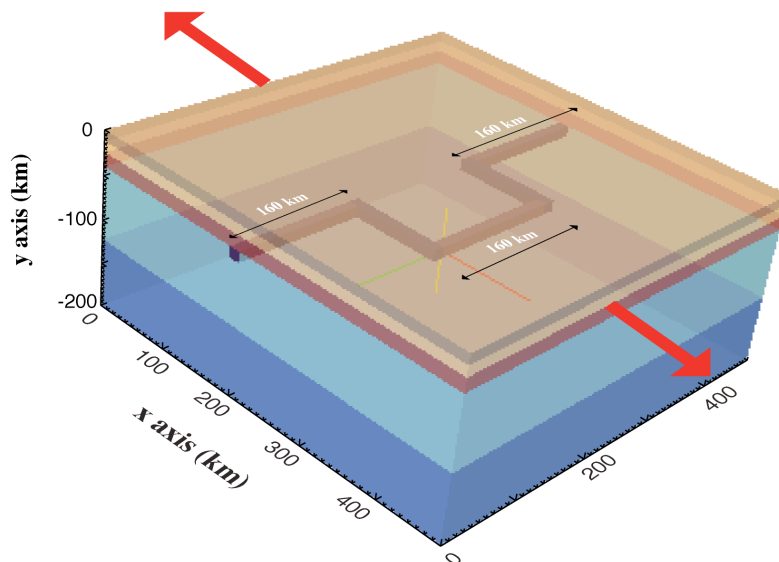

Figure 18: *Numerical setup for lithosphere-scale extension with an irregular rift shape. Three seeds (each 160 km long) run parallel to the z-axis and are connected by seeds that are not as "weak." These two connecting seeds approximate the transfer faults between the offset rifts. Rheological properties for this experiment are the same as for the 2-D experiments (Table 1).*
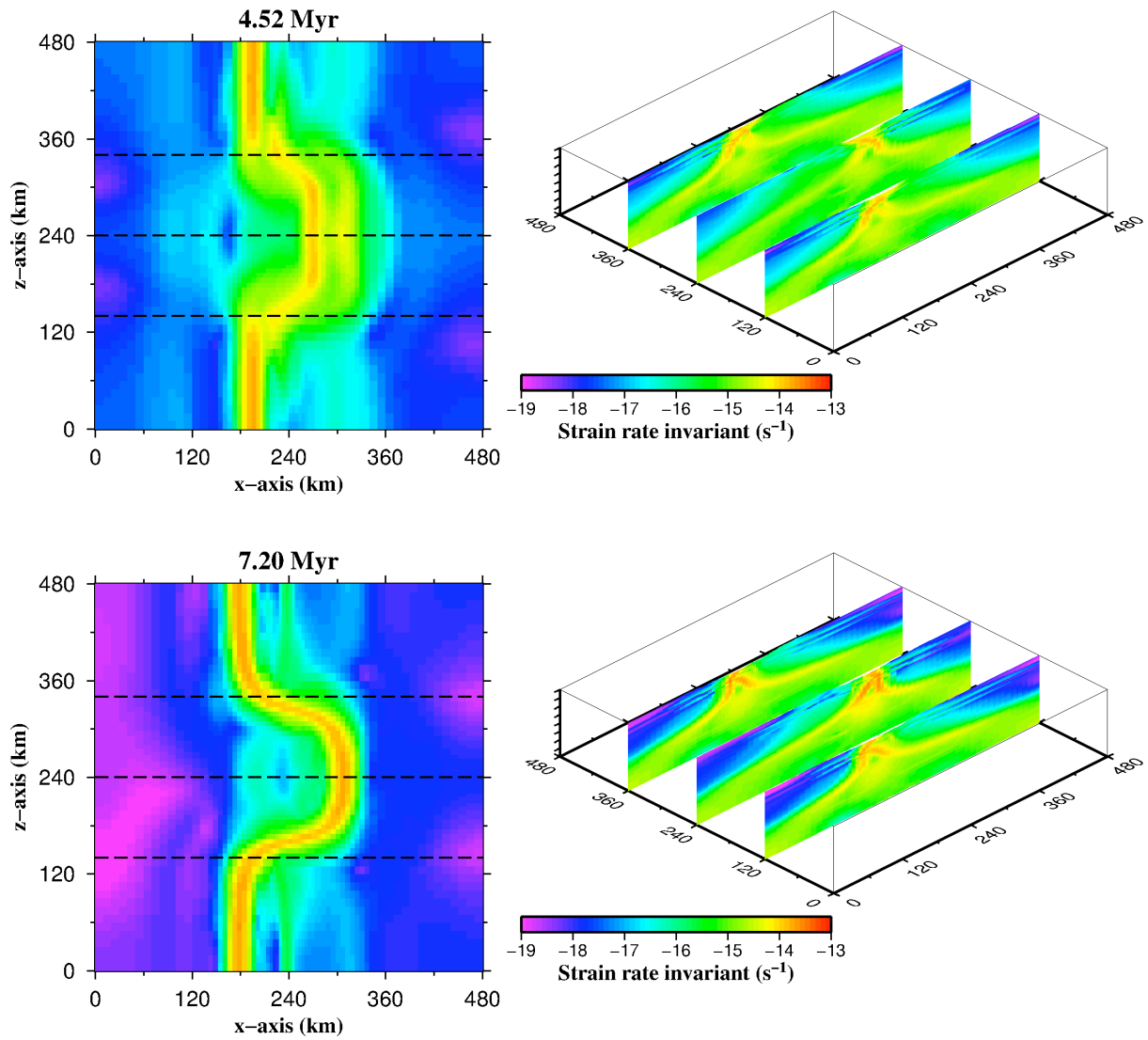
Figure 19: *Numerical results for extension in the upper and lower crust after 4.5 Myr (Top) and 7.2 Myr (Bottom) for the setup in Figure 18. The vertical axis in the 3-D plots (Right) is scaled by a factor of 0.48. In comparison to the crustal-scale 3-D models, deformation focuses only in the regions of the seeds. The two rifts on the left side of the model do not propagate and connect because of the transfer zone seeds connecting them to the seed on the right side of the model. This 3-D model by J. Tetreault and S. Buiter.*

5.3 Continental extension with inherited structure and hot (plume-derived) material

The simple models with inherited structure (*Sections 5.1 and 5.2*) illustrate that extension and continental break-up will not easily jump to adjacent areas once seafloor spreading has localised in a region. Yamasaki and Gernigon (2010) show how instantaneous emplacement of hot regions in the uppermost lithospheric mantle may allow an active rift to jump and thus produce a microcontinent. However, in this type of models a microcontinent is only produced for very specific combinations of the temperature difference and time offset between the emplaced temperature anomalies. The results of Yamasaki and Gernigon (2010) illustrate that extension can only migrate laterally if the new future centre of extension is weak enough in comparison with the rift that needs to be abandoned. We use the insight obtained by the models of Yamasaki and Gernigon (2010) to show how a microcontinent can be produced in a dynamic rift model with instantaneous emplacement of a large hot body (*Figs. 20 and 21*).

For this experiment we employ a lithospheric strength profile for a continent with a strong lower crust (gabbro). In this setup (*Fig. 20*), the middle crust contains a thick ductile layer, which serves to isolate a crustal block between two zones of deformation, thus creating a continental fragment on one margin. This initial crustal rheology allows for two rifts to be created from one initial pre-existing weakness. These two rifts will isolate a crustal body that will eventually evolve into a continental fragment on one margin. For the extra factor needed to produce a microcontinent from a continental fragment, we emplace a hot body under the failed basin on the margin with the continental fragment to re-initiate rifting in that basin.

The timing of emplacement and the amount of heat emplaced is important, as noted by Yamasaki and Gernignon (2010). If the hot body is not significantly hotter than the country rock, the failed rift will not re-initiate. If the hot body is emplaced before the successful rift evolves fully to break-up, the failed rift will re-initiate and the previously successful rift will be abandoned before going to break-up. In *Figure 20* we show an experiment where the emplacement temperature and timing has led to the successful creation of a microcontinent.

Without emplacement of a hot body, such as a large magmatic crustal intrusion, the model will evolve to one margin with a small continental fragment and another margin with hyper-extended crust (*Fig. 20a,c*). If a hot body under the failed rift is emplaced after crustal break-up, here ca. 100 Myr, the failed rift separating the continental fragment from the mainland is re-initiated (*Figs. 20d and 21*). Emplacement of a hot body will shift the location of deformation almost geologically instantaneously because the failed basin has an already weakened and thinned crust and mantle. Therefore, we can conclude that initial rifting in the two basins can be concurrent, but final break-up under the two separate basins is not.

A fast jump in rift location agrees with the scenario for Jan Mayen, where the Kolbeinsey Ridge became active around the time at which the Aegir Ridge was abandoned, although in our model break-up on the left ridge is delayed. In the simple model we instantaneously emplaced a hot region. In the next Section we test whether dynamic emplacement of molten, hot material by plume impingement might create a microcontinent.
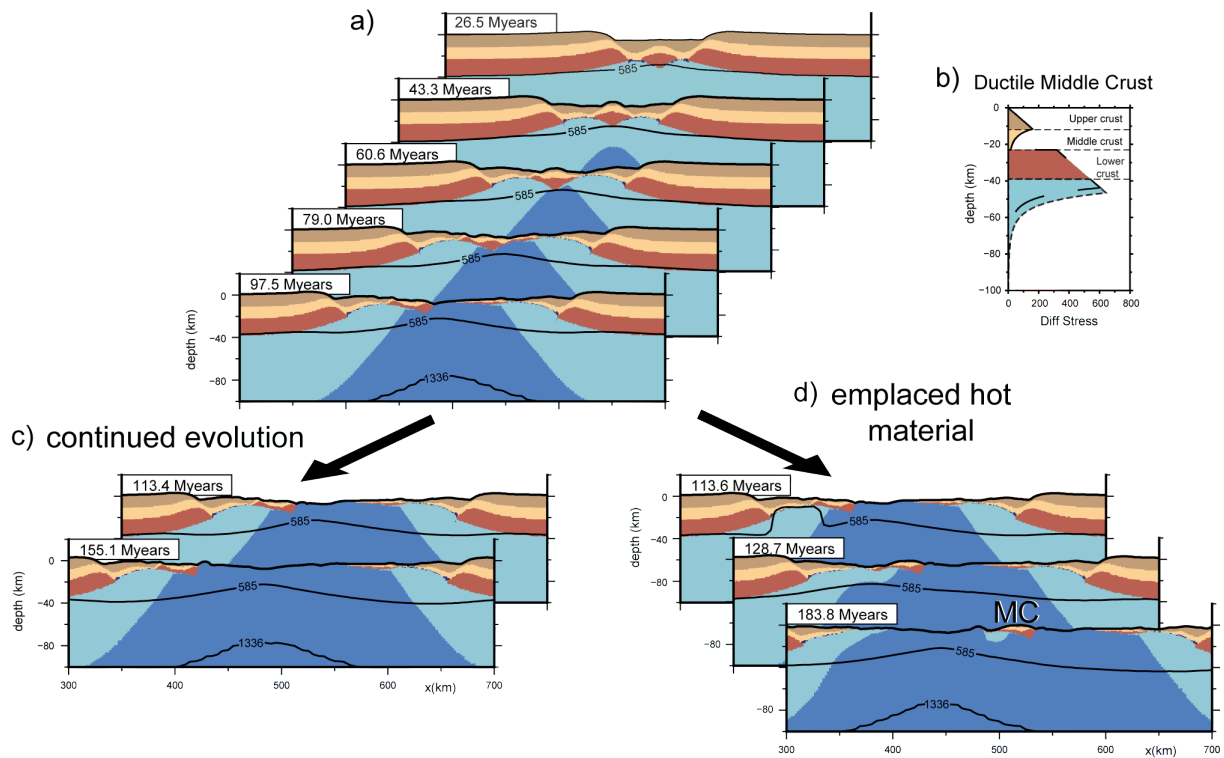
Figure 20: *Two models showing the effects of inheritance and emplaced hot material. a) Model evolution until 97.5 Myr for a model with one inherited seed initially at x = 500 km, just below the Moho. The ultraslow extension distributes crustal thinning, leading initially to the formation of two rifts. Crustal break-up occurs at the right rift at ca. 100 Myr. c) Continued evolution of the model with inheritance until 155 Myr shows that an ocean opens and a continental fragment is produced, but no microcontinent. d) When hot material is emplaced in the left rift at 113 Myr (T = 1100 °C, at x = 390-430 km and depths -10 to -45 km), break-up is then also produced in the left rift at ca. 160 Myr, creating a microcontinent (MC). Full extension rate is 0.2 cm/yr. Initial strength of the materials is shown in b). The lower crust follows a gabbro flow law (Zhou et al., 2012).*
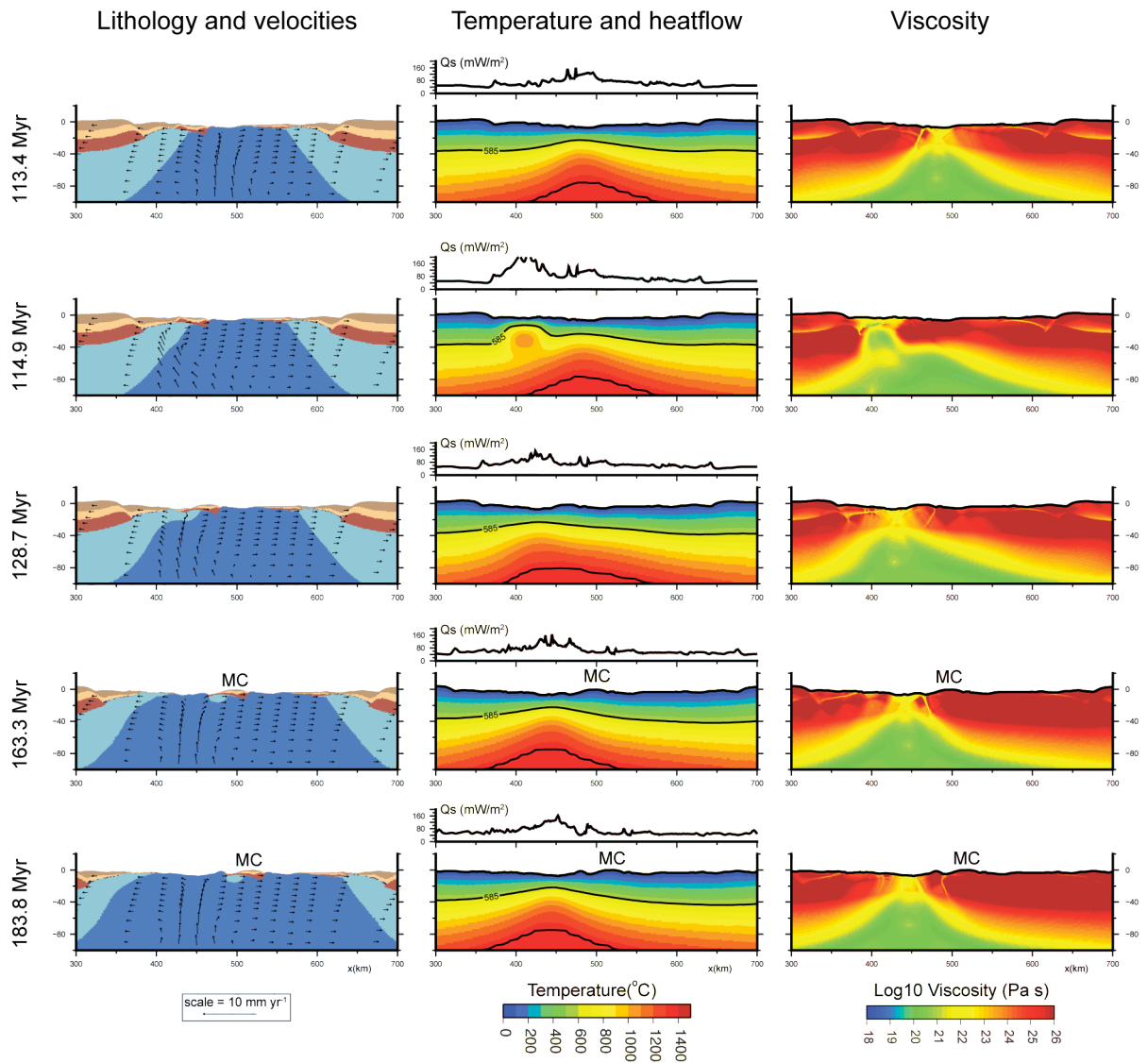
Figure 21*: Detailed evolution of the centre part of the model of Figure 20a and d. Rifting initiates at one inherited weak region and hot material is emplaced instantaneously at 113 Myr. a) Lithology and velocity field, b) temperature and surface heatflow, and c) viscosities. MC = microcontinent.*

5.4 Extension of models with inherited structure and an impacting plume

While emplacing a hot body after the passive margin has evolved (*Section 5.3*) provides us with some understanding of timing of rifting events, the emplacement does not occur dynamically. In order to dynamically produce a hot intrusive body under the failed rift, a plume is necessary.

To simulate this scenario (scenario 6 in *Chapter 1*), we take the same initial setup as in *Section 5.1*, but introduce a plume that is offset from the two seeds (*Fig. 22*). The two seeds in this experiment do not have the same rheological property: seed 1 is 'stronger' than seed 2. This difference is necessary so that the rift furthest from the plume will initiate and continue. Without this difference in the rheological strength, the uprising plume would always cause the rift nearest to it to go to break-up and the farthest seed would not initiate rifting. Thus, our setup forces a rift to be created and evolve to break-up before an offset plume impinges on the lithosphere. The plume is initiated at the start of the model, by a semi-circle at the base of the model with a temperature of 1627 ºC (ΔT = 200 ºC from the base of the model).
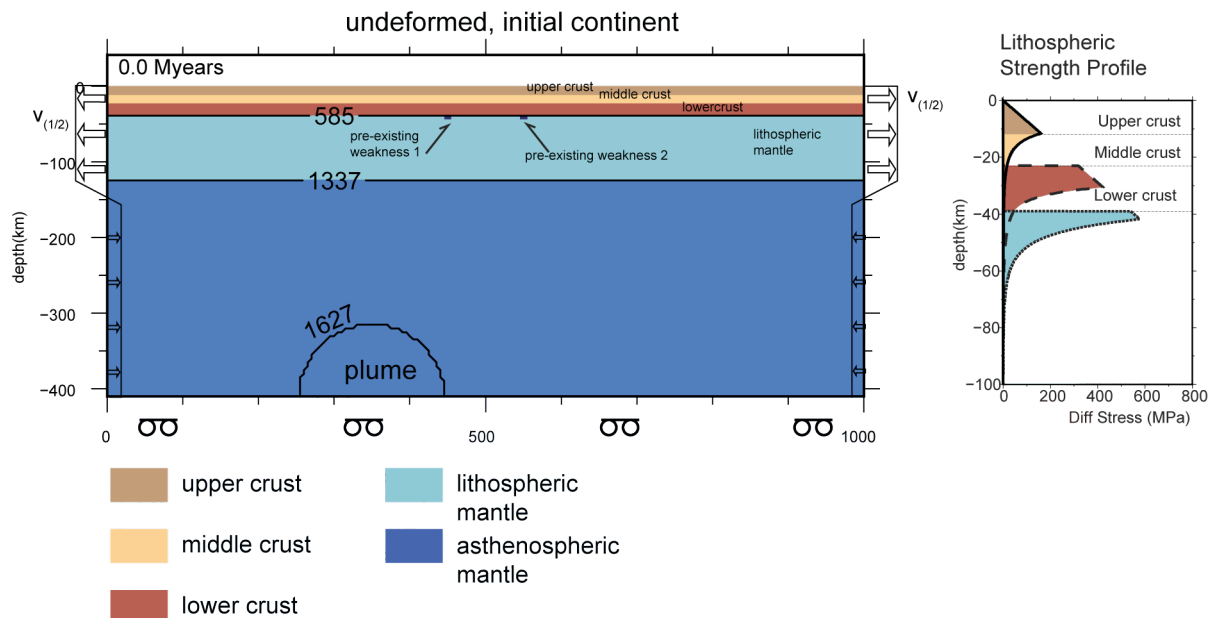

Figure 22*. Numerical setup for the experiment with two seeds and a plume. The model uses crustal rheology setup 2 of Tetreault and Buiter (in prep.). This setup is identical as that for the experiment in Section 5.1 (Figs. 12, 13) except one seed is rheologically stronger than the other and a plume is initiated at the base of the model.*

This experiment initially evolves in a similar manner to the model described in *Section 5.1*. Both seeds initiate rifts, but the rift farthest away from the plume (at pre-existing weakness 2) evolves farther to continental break-up (*Fig. 23a*). The left rift (at pre-existing weakness 1) fails after ca. 9 Myr. During passive margin rifting, the plume rises. Once the hot plume material rises to a depth shallow enough to produce decompression melting, mantle melt starts rising into the lithosphere above the plume (*Fig. 23b-c*). The melt eroding the lithosphere helps to focus the direction of the rising plume (*Fig. 23c*). It should be noted that without melt processes, the plume would be deflected toward the already evolved rift, and no microcontinent would be formed (*Fig. 24*). The buoyancy and heat from the rising plume melt cause the left rift to re-initiate once the melt has reached the crust (*Fig. 23d*). Once the rift above the plume re-initiates, the extension in the other rift (now seafloor spreading) ceases

(*Fig. 23d*). Rifting continues above the plume and continental break-up and seafloor spreading will follow in this location. By the end of the experiment at 17 Myears, both rifts show high surface heat flow (*Fig. 25*).

Some notable results from this experiment are the timing of rift-initiation and the crustal thickness of the microcontinent. Once the plume is at a depth to produce melt (close to lithospheric depth), rifting and break-up occurs quite rapidly. The magmatic bodies are emplaced below the crust and lead to break-up within 2 Myr. This is more rapid than the time for rift re-initiation and break-up in the experiment in *Section 5.3,* which took ca. 47 Myr to go from re-initiation to break-up. The reason behind the more rapid break-up with a plume is that in this experiment, hot magma is regularly being emplaced under the crust while in *Section 5.3*, there was only one pulse of magmatism simulated. The almost instantaneous shift of rift activity of the right rift to the plume-induced left rift is similar to the tectonic setting for Jan Mayen, where the Aegir Ridge was abandoned by ca. 30 Ma when rifting jumped to the Kolbeinsey Ridge. Seafloor spreading between Jan Mayen and Greenland initiated by 25 Ma (or earlier) and was complete by ca. 23-20 Ma (*Chapter 3*), indicating a slightly longer time to achieve break-up in the re-initiated rift than we achieve in the models. This is likely caused by the strong focusing effect that the melt has in our models. Perhaps a successful scenario of Jan Mayen formation should include one pulse of melt migration and some amount of lateral plume flow.
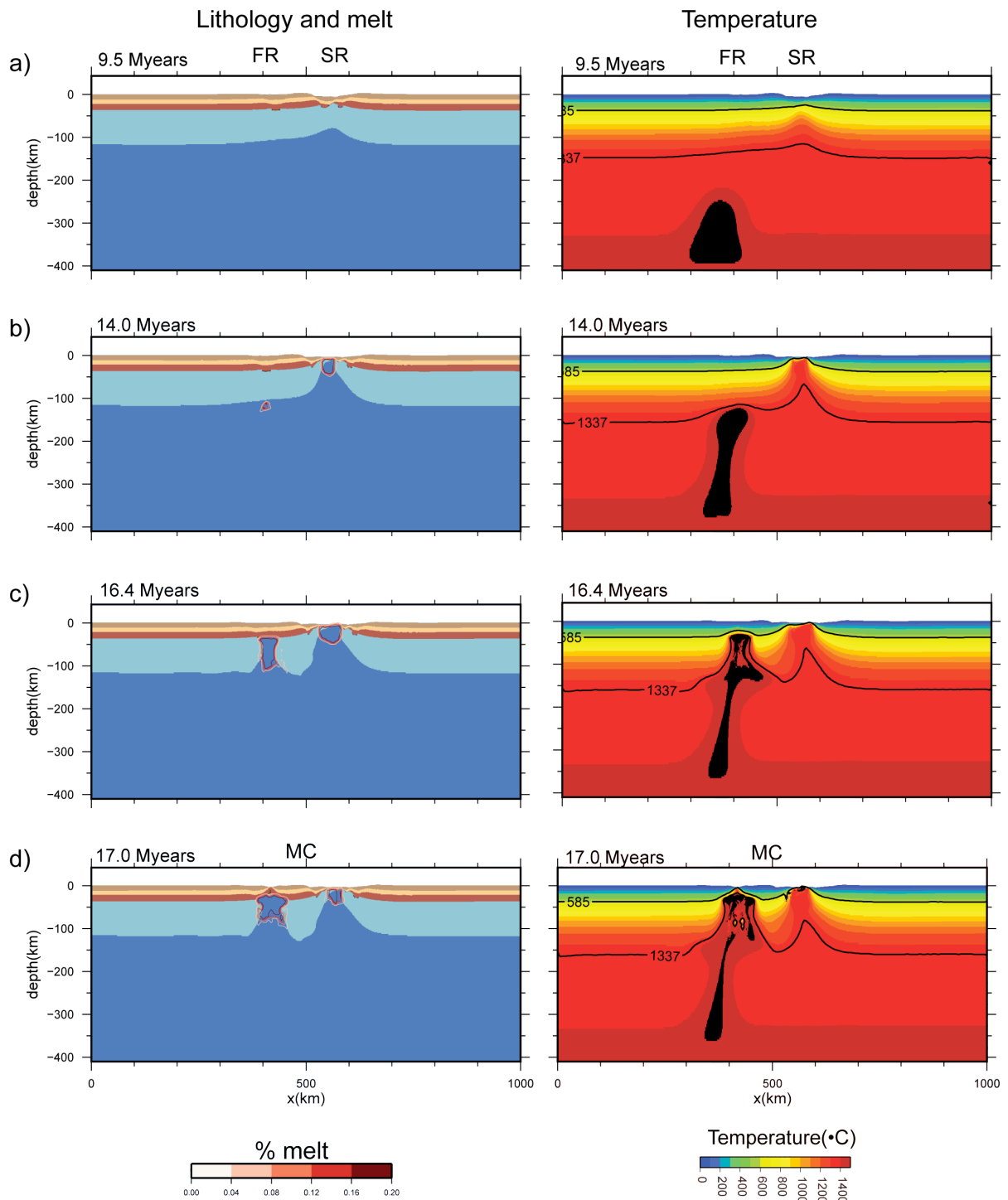
Figure 23*: Evolution of model with a plume and two rifts. (a) After ca. 9 Myr the left rift fails (FR=failed rift) and the right rift continues (SR=successful rift). (b) The plume continues to rise but does not affect the ongoing rift, which continues to break-up around 14 Myr. (c) The plume begins to impinge into the lithosphere under the FR and emplace melt below the crust. (d) After enough hot magma has been emplaced under the crust of the FR, the FR re-initiates (ca. 17 Myr) and deformation jumps to this location, abandoning seafloor spreading at the SR. MC=microcontinent. The evolution of surface topography and heat flow is shown in Figure 25.*
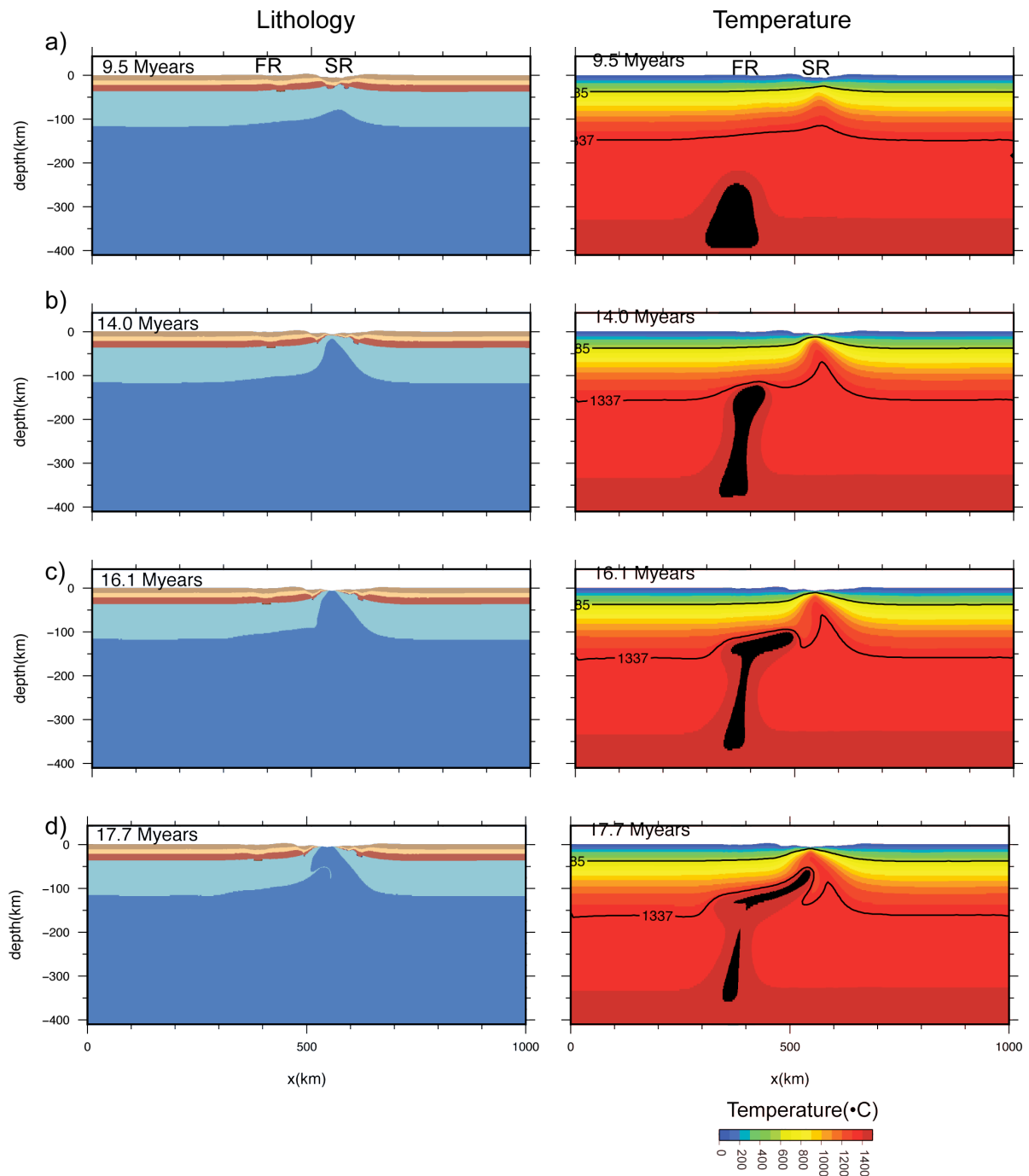
Figure 24: *Evolution of model with plume and two rifts, but no melt processes. (a) After ca. 9 Myr the left rift fails (FR=failed rift) and the right rift continues (SR=successful rift). (b) The plume continues to rise, but does not affect the ongoing rift, which continues to break-up around 14 Myr. (c) The plume begins to impinge into the lithosphere under the FR and is being deflected towards the SR. (d). Plume material flows into the seafloor spreading SR. No microcontinent is produced.*

Another important result is that the microcontinent crust in this experiment has undergone virtually no thinning and has narrow margins. This crustal structure is similar to that of Seychelles, which has a crustal thickness of 39 km, similar to that of mainland India. Whereas for Jan Mayen, the crustal thickness varies from 7 to 24 km, indicating significant thinning occurred prior to plume-related break-up.

The plume does not create significant disturbances to the surficial topography or heatflow until the overlying lithosphere has been thinned (*Fig. 25*). Magmatic underplating of the thick continental crust (*Fig. 23c*) does produce a minor uplift from the buoyant melt, but the surface heat flow remains low (*Fig. 25c*). In our geodynamic models, melt does not migrate laterally significantly during underplating, thus leaving underplated magma only at the margins and not under the microcontinent.
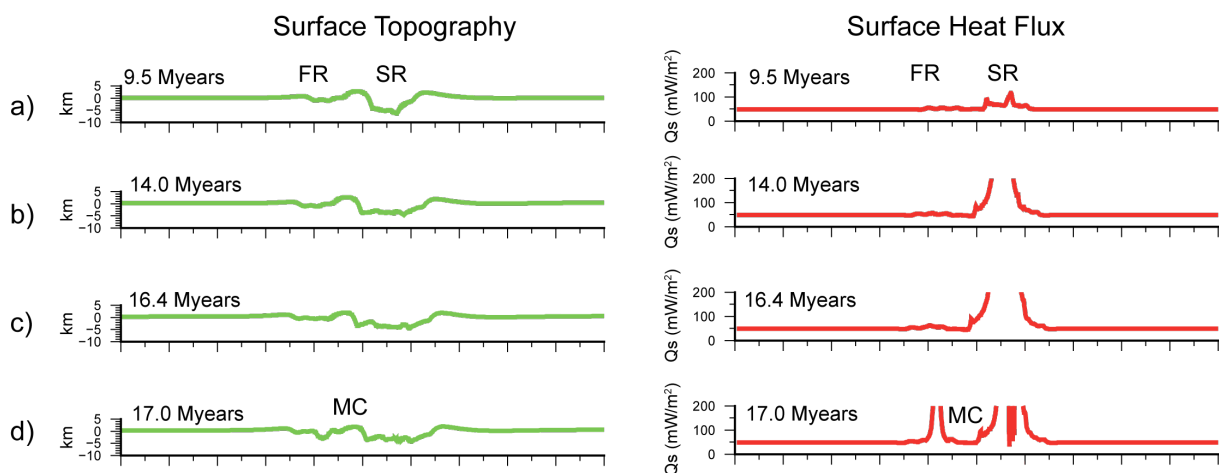

Figure 25: *Evolution of surface topography and heat flow for the model with a plume, two rifts, and melt (Fig. 23). (a) After ca. 9 Myr the left rift fails (FR=failed rift) and the right rift continues (SR=successful rift). (b-c) The plume continues to rise but does not affect the overlying topography or heat flow. (d) The plume-related melt that has underplated the FR initiates rifting and break-up, which is reflected in the topography and heat flow. MC=microcontinent.*

6. CONCLUSIONS

The formation of the Jan Mayen microcontinent represents an intriguing mechanical challenge because of the difficulty to initiate continental break-up in a new location at the Kolbeinsey Ridge once seafloor spreading was already underway at the Aegir Ridge. Based on a review of the present literature, we arrived at the following scenario for the evolution of the Jan Mayen microcontinent:

(1)   Parts of proto-Jan Mayen were involved in the Caledonide collision (430–420 Ma), creating heterogeneous crustal and lithospheric lithologies with inherited shear zones.
(2)   Rifting between Norway and Greenland occurred in several phases from the Carboniferous onwards. Also the crustal blocks of Jan Mayen underwent some amount of extension during this time.
(3)   Seafloor spreading on the Aegir Ridge started 55–53 Ma, separating Jan Mayen from Norway.
(4)   The Aegir Ridge was abandoned at some time between 34–25 Ma. Since the last stages of rifting were ultraslow and disorganised, we place cessation of rifting at ca. 30 Ma.
(5)   Rifting jumped to the Kolbeinsey Ridge on the western side of Jan Mayen at ca. 25–24 Ma or earlier. Break-up on the Kolbeinsey ridge was complete by ca. 23–20 Ma, isolating the Jan Mayen microcontinent.
(6)   The North Atlantic Igneous Province, initiated at 63–61 Ma, has been related to the Iceland Plume. The hotspot (fixed or mobile) was in a location directly west of future Jan Mayen from ca. 40–30 Ma.

Structurally, Jan Mayen is composed of a few continental crustal blocks, including the Jan Mayen Ridge and the Southern Ridge complex. The Jan Mayen Ridge is less then 100 km wide. The crustal thickness of Jan Mayen varies between 7 and 24 km, excluding sediments. The eastern margin of Jan Mayen is classified as magmatic, based on intrusions in the sedimentary sequences, seaward dipping reflectors, and possible magmatic underplating. The western margin is usually considered non-magmatic, but does have sill-like intrusions in the sedimentary layers and a thicker than average oceanic crust, which point to a mantle-melt influence.

We used numerical models to test formation of the Jan Mayen microcontinent by localisation on inherited structure, potentially enhanced by warm material of the Iceland Plume. Our models show that a plume is needed to shift the locale of deformation from seafloor spreading to continental crust in extension. Once hot material from a plume is emplaced into the lithosphere, re-initiation of the failed rift and the ensuing time to break-up is rapid (a few Myr). The rapid break-up time due to magmatic underplating leads to a microcontinent that has narrow margins and a relatively unthinned crust.

The Jan Mayen microcontinent has a crust that varies in thickness and is covered by pre-Cretaceous to Cenozoic sediments, which suggests that Jan Mayen has undergone an earlier extension stage, similar to when a continental fragment is produced in an ultraslow rift setting, prior to the plume-related break-up from Greenland. We have shown through geodynamic experiments that the extension rate and the crustal rheology of the extending continent will both play important roles in producing continental fragments on passive margins. We propose that Jan Mayen was produced by two stages. First, rifting between Greenland and Norway led to Jan Mayen existing as a continental fragment on the Greenland margin. Second, the Iceland plume produced the necessary process to reinitiate the failed rift between Jan Mayen and Greenland and rapidly separate the two. The western Jan Mayen

margin would then have undergone two major pulses of heat flow and uplift due to rifting, the first pulse related to the extension phase that led to break-up between Jan Mayen and Norway and the second pulse related to re-initiation of rifting after emplacement of magma by the Iceland plume leading to break-up between Jan Mayen and Greenland.

Our geodynamic experiments with a plume indicate that melt migration will focus strain in the mantle and therefore direct the plume upwards into relatively undeformed continental crust. On the other hand, our experiment with a plume and no melt shows that the plume will flow laterally at the base of the lithosphere towards the location with ongoing seafloor spreading. In the Jan Mayen-Greenland-Norway system, there are voluminous amounts of magmatic material on the Norwegian margin, but geophysical observations point to only limited amounts of magmatic material on Jan Mayen's margins. From our two plume models, we infer that the Iceland plume flowed laterally below the Greenland-Jan Mayen lithosphere before producing melt that focused deformation to break up Jan Mayen from Greenland.

Acknowledgements

REFERENCES

Armitage, J.J., J.S. Collier, T.A. Minshull, T.J. Henstock, 2011. Thin oceanic crust and flood basalts: India-Seychelles breakup. Geochemistry, Geophysics, Geosystems 12, Q0AB07, doi: 10.1029/2010GC003316

Asimow, P. D., J. E. Dixon, and C. H. Langmuir, 2004. A hydrous melting and fractionation model for mid-ocean ridge basalts: Application to the Mid-Atlantic Ridge near the Azores. Geochemistry. Geophysics, Geosystems 5, Q01E16, doi: 10.1029/2003GC000568.

Bernard, A., Munschy, M., 2000. Le bassin des Mascareignes et le bassin de Laxmi (ocean Indien occidental) se sont-ils formés à l'axe d'unmême centre d'expansion? Comptes Rendus de l'Academie des Sciences Paris, Sciences de la Terre et de planètes 330, 777–783

Blankenbach, B., F. Busse, U. Christensen, L. Cserepes, D. Gunkel, U. Hansen, H. Harder, G. Jarvis, M. Koch, G. Marquart, D. Moore, P. Olsen, H. Schmeling, T. Schnaubelt, 1989. A benchmark comparison for mantle convection codes. Geophysical Journal International 98, 23-38

Bos, B., C.J. Spiers, 2002. Frictional-viscous flow of phyllosilicate bearing fault rock: Microphysical model and implications for crustal strength profiles. Journal of Geophysical Research 107 (B2), 2028, doi: 10.1029/2001JB000301

Braun, J., 1992. Postextensional Mantle Healing and Episodic Extension in the Canning Basin. Journal of Geophysical Research 97, 8927-8936

Breivik, A.J., R. Mjelde, J.I. Faleide, Y. Murai, 2006. Rates of continental breakup magmatism and seafloor spreading in the Norway Basin–Iceland plume interaction. Journal of Geophysical Research 111, B07102, doi: 10.1029/2005JB004004

Brekke, H., R.W. Williams, C. Magnus, 2008. The Geology of the Norwegian Sea Continental Margin and Probable Similarities with the Jan Mayen Ridge. First Petroleum Exploration Conference in Iceland, Reykjavík, 4-5 September 2008

Buiter, S.J.H., T.H. Torsvik, 2014. A review of Wilson Cycle plate margins: A role for mantle plumes in continental break-up along sutures? Gondwana Research 26, 627-653, doi: 10.1016/j.gr.2014.02.007

Christensen, N.I., W.D. Mooney, 1995. Seismic velocity structure and composition of the continental crust: A global view. Journal of Geophysical Research 100, 9761-9788

Coffin, M.F., O. Eldholm, 1992. Volcanism and continental break-up: a global compilation of large igneous provinces. Geological Society, London, Special Publications 68, 17030, doi: 10.1144/GSL.SP.1992.068.01.02

Coffin, M.F., P.D. Rabinowitz, 1988. Evolution of the conjugate East African–Madagascar margins and western Somali Basin. Special Papers Geological Society of America 226, 77pp.

Collier, J.S., V. Sansom, O. Ishizuka, R.N. Taylor, T.A. Minshull, R.B. Whitmarsh, 2008. Age of Seychelles–India break-up. Earth and Planetary Science Letters 272, 264–277

Courtillot, V.E., P.R. Renne, 2003. On the ages of flood basalt events. Comptes Rendus Geosciences 335, 113–140, doi: 10.1016/S1631-0713(03)00006-3

Crameri, F., H. Schmeling, G.J. Golabek, T. Duretz, R. Orendt, S.J.H. Buiter, D.A. May, B.J.P. Kaus, T.V. Gerya, P.J. Tackley, 2012. A comparison of numerical surface topography calculations in geodynamic modelling: An evaluation of the 'sticky air'

method. Geophysical Journal International 189, 38-54, doi: 10.1111/j.1365-246X.2012.05388.x

Cuvelier, C., A. Segal, A.A. van Steenhoven, 1986. Finite Element Methods and Navier-Stokes Equations, D. Reidel Publishing Company, Dordrecht, Holland, 483 pp.

Doré, A.G., 1991. The structural foundation and evolution of Mesozoic seaways between Europe and the Arctic. Palaeogeography, Palaeoclimatology, Palaeoecology 87, 441-492

Eagles, G., R. Gloaguen, C. Ebinger, 2002. Kinematics of the Danakil microplate. Earth and Planetary Science Letters 203, 607-620

Ellis, S.M., T.A. Little, L.M. Wallace, B.R. Hacker, S.J.H. Buiter, 2011. Feedback between rifting and diapirism can exhume ultrahigh-pressure rocks. Earth and Planetary Science Letters 311, 427-438, doi: 10.1016/j.epsl.2011.09.031

Escartin, J., G. Hirth, B. Evans, 1997. Effects of serpentinization on the lithospheric strength and the style of normal faulting at slow-spreading ridges. Earth and Planetary Science Letters 151,181-189

Foulger, G.R., 2006. Older crust underlies Iceland. Geophysical Journal International 165, 672-676, doi: 10.1111/j.1365-246X.2006.02941.x

Fullsack, P., 1995. An arbitrary Lagrangian–Eulerian formulation for creeping flows and its applications in tectonic models. Geophysical Journal International 120, 1–23, doi: 10.1111/j.1365-246X.1995.tb05908.x

Furlong, K. P., D.M. Fountain, 1986. Continental crustal underplating: Thermal considerations and seismic-petrologic consequences. Journal of Geophysical Research 91, 8285–8294, doi: 10.1029/JB091iB08p08285.

Gaina, C., R.D. Müller, B.J. Brown, T. Ishihara, 2003. Microcontinent formation around Australia. Geological Society of America Special Papers 372, 405-416, doi: 10.1130/0-8137-2372-8.405

Gaina, C., L. Gernigon, P. Ball, 2009. Palaeocene–Recent plate boundaries in the NE Atlantic and the formation of the Jan Mayen microcontinent. Journal of the Geological Society London 166, 601-616, doi: 10.1144/0016-76492008-112

Ganerød, M., M.A. Smethurst, T.H. Torsvik, T. Prestvik, S. Rousse, C. McKenna, D.J.J. van Hinsbergen, B.W.H. Hendriks, 2010. The North Atlantic Igneous Province reconstructed and its relation to the Plume Generation Zone: the Antrim Lava Group revisited. Geophysical Journal International 182, 183-202, doi: 10.1111/j.1365-246X.2010.04620.x

Ganerød, M., T.H. Torsvik, D.J.J. van Hinsbergen, C. Gaina, F. Corfu, S. Werner, T.M. Owen-Smith, L.D. Ashwal, S.J. Webb, B.W.H. Hendriks, 2011. Palaeoposition of the Seychelles microcontinent in relation to the Deccan Traps and the Plume Generation Zone in Late Cretaceous–Early Palaeogene time. In D.J.J. van Hinsbergen, S.J.H. Buiter, T.H. Torsvik, C. Gaina, S.J. Webb eds., The Formation and Evolution of Africa: A Synopsis of 3.8 Ga of Earth History. Geological Society, London, Special Publications 357, 229–252, doi: 10.1144/SP357.12

Gernigon, L., C. Gaina, O. Olesen, P.J. Ball, G. Péron-Pinvidic, T. Yamasaki, 2012. The Norway Basin revisited: From continental breakup to spreading ridge extinction. Marine and Petroleum Geology 35, 1-19, doi: 10.1016/j.marpetgeo.2012.02.015

Gerya, T.V., 2013. Three-dimensional thermomechanical modeling of oceanic spreading initiation and evolution, Physics of the Earth and Planetary Interiors 214, 35–52, doi: 10.1016/j.pepi.2012.10.007

Ghazian, R.K. S.J.H. Buiter, 2013. A numerical investigation of continental collision styles. Geophysical Journal International 193, 1133-1152, doi: 10.1093/gji/ggt068

Ghazian, R.K., S.J.H. Buiter, 2014. Numerical modelling of the role of salt in continental collision: An application to the southeast Zagros fold-and-thrust belt. Tectonophysics 632, 96-110, doi: 10.1016/j.tecto.2014.06.006

Ghods, A., J. Arkani-Hamed, J., 2000. Melt migration beneath mid-ocean ridges. Geophysical Journal International 140, 687–697, doi: 10.1046/j.1365-246X.2000.00032.x

Greenhalgh, E.E., N.J. Kusznir, 2007. Evidence for thin oceanic crust on the extinct Aegir Ridge, Norwegian Basin, NE Atlantic derived from satellite gravity inversion. Geophysical Research Letters 34, L06305, doi: 10.1029/2007GL029440

Grove, T. L., R. J. Kinzler, W. B. Bryan, 1992. Fractionation of mid-ocean ridge basalt (MORB), in Mantle Flow and Melt Generation at Mid-Ocean Ridges. Geophysical Monograph Series 71, 281–310. AGU, Washington, DC

Gudlaugsson, S.T., K. Gunnarsson, M. Sand, J. Skogseid, 1988. Tectonic and volcanic events at the Jan Mayen Ridge microcontinent. In A.C. Morton, L.M. Parson, eds., Early Tertiary Volcanism and the Opening of the NE Atlantic. Geological Society Special Publication 39, 85-93

Hansen, J., D.A. Jerram, K. McCaffrey, S.R. Passey, 2009. The onset of the North Atlantic Igneous Province in a rifting perspective. Geological Magazine 146, 309-325, doi: 10.1017/S0016756809006347

Hirth, G., C. Teyssier, J. Dunlap, 2001. An evaluation of quartzite flow laws based on comparisons between experimentally and naturally deformed rocks. International Journal of Earth Sciences 90, 77–87

Hirth, G., S. Guillot, 2013. Rheology and tectonic significance of serpentinite. Elements 9, 107-113, doi: 10.2113/gselements.9.2.107

Jung, W.-Y., P.R. Vogt, 1997. A gravity and magnetic anomaly study of the extinct Aegir Ridge, Norwegian Sea. Journal of Geophysical Research 102, 5065-5089

Katz, R. F., M. Spiegelman, M., C.H. Langmuir, 2003. A new parameterization of hydrous mantle melting. Geochemistry, Geophysics, Geosystems 4, doi: 10.1029/2002GC000433

Kaus, B.J.P., H. Mühlhaus, D.A. May, 2010. A stabilization algorithm for geodynamic numerical simulations with a free surface. Physics of the Earth and Planetary Interiors 181, 12-20, doi: 10.1016/j.pepi.2010.04.007

Kelemen, P. B., G. Hirth, N. Shimizu, M. Spiegelman, H.J. Dick, 1997. A review of melt migration processes in the adiabatically upwelling mantle beneath oceanic spreading ridges. Philosophical Transactions of the Royal Society of London. Series A: Mathematical, Physical and Engineering Sciences 355, 283–318

Kodaira, S., R. Mjelde, K. Gunnarsson, H. Shiobara, H. Shimamura, 1998. Structure of the Jan Mayen microcontinent and implications for its evolution. Geophysical Journal International 132, 383-400

Kohlstedt, D. L., B. K. Holtzman, 2009. Shearing melt out of the earth: An experimentalist's perspective on the influence of deformation on melt extraction. Annual Review of Earth and Planetary Sciences 37(1), 561–593

Lacroix, B., T. Tesei, E. Oliot, A. Lahfid, C. Collettini, 2015. Early weakening processes inside thrust faults. Tectonics in press, doi: 10.1002/2014TC003716

Lawver, L.A., R.D. Müller, 1994. Iceland hotspot track, Geology 22, 311-314

Lundin, E.R., A.G. Doré, 2011. Hyperextension, serpentinization, and weakening: A new paradigm for rifted margin compressional deformation. Geology 39, 347-350, doi: 10.1130/G31499.1

Mandl, G., 1988. Mechanics of Tectonic Faulting: Models and Basic Concepts. Elsevier Science, Amsterdam, Netherlands, 407 pp.

McKenzie, D. 1984. The Generation and Compaction of Partially Molten Rock. Journal of Petrology 25, 713–765, doi: 10.1093/petrology/25.3.713.

Mei, S., W. Bai, T. Hiraga, D.L. Kohlstedt, 2002. Influence of melt on the creep behavior of olivine-basalt aggregates under hydrous conditions. Earth and Planetary Science Letters 201, 491–507, doi: 10.1016/S0012-821X(02)00745-8

Mével., C., 2003. Serpentinization of abyssal peridotites at mid-ocean ridges. C.R. Geoscience 335, 825-852, doi: 10.1016/j.crte.2003.08.006

Meyer, R., J. van Wijk, L. Gernigon, 2007. The North Atlantic Igneous Province: A review of models for its formation. In Foulger, G.R., and Jurdy, D.M., eds., Plates, plumes, and planetary processes, Geological Society of America Special Paper 430, 525–552, doi: 10.1130/2007.2430(26)

Mihalffy, P., B. Steinberger, H. Schmeling, 2008. The effect of the large-scale mantle flow field on the Iceland hotspot track. Tectonophysics 447, 5-18, doi: 10.1016/j.tecto.2006.12.012

Mittelstaedt, E., G. Ito, J. van Hunen, 2011. Repeat ridge jumps associated with plume-ridge interaction, melt transport, and ridge migration. Journal of Geophysical Research 116, B01102, doi: 10.1029/2010JB007504

Mjelde, R., T. Raum, A.J. Breivik, J.I. Faleide, 2008. Crustal transect across the North Atlantic. Marine Geophysical Researches 29, 73-87, doi: 10.1007/s11001-008-9046-9

Müller, R.D., W.R. Roest, J.-Y. Royer, L.M. Gahagan, J.G. Sclater, 1997. Digital isochrons of the world's ocean floor. Journal of Geophysical Research 102, 3211–3214

Müller, R.D., C. Gaina, W.R. Roest, D.L. Hansen, 2001. A recipe for microcontinent formation. Geology 29, 203-206

Müller, R.D., M. Sdrolias, C. Gaina, W.R. Roest, 2008. Age, spreading rates, and spreading asymmetry of the world's ocean crust. Geochemistry, Geophysics, Geosystems 9, Q04006, doi: 10.1029/2007GC001743

Naliboff, J., S.J.H. Buiter, 2015. Rift reactivation and migration during multiphase extension. Earth Planetary Science Letters 421, 58-67, doi: 10.1016/j.epsl.2015.03.050

Naylor, D., P. Shannon, 2005. The structural framework of the Irish Atlantic Margin. In Doré, A.G., B.A. Vining, eds., Petroleum Geology: North-West Europe and Global Perspectives - Proceedings of the 6th Petroleum Geology Conference, Geological Society, London, 1009–1021, doi:10.1144/0061009

Norwegian Petroleum Directorate, 2013. Petroleum resources on the Norwegian continental shelf, 2013 exploration. http://www.npd.no/Global/Engelsk/3-Publications/Resource-report/Resource-report-2013/Ressursrapport-2013-eng.pdf

Nunns, A.G., 1983. Plate tectonic evolution of the Greenland-Scotland Ridge and surrounding regions. In M.H.P. Bott, S. Saxov, M. Talwani, J. Thiede, eds., Structure and Development of the Greenland - Scotland Ridge: New Methods and Concepts, Springer, New York, 11-30

Ottemöller, L., V. Midzi, 2003. The crustal structure of Norway from inversion of teleseismic receiver functions. Journal of Seismology 7, 35-48

Pelletier, D., A. Fortin, R. Camarero, 1989. Are FEM solutions of incompressible flows really incompressible? (Or how simple flows can cause headaches!). International Journal Numerical Methods in Fluids 9, 99-112

Péron-Pinvidic, G., G. Manatschal, 2010. From microcontinents to extensional allochthons: witnesses of how continents rift and break apart? Petroleum Geoscience 16, 189–197, doi: 10.1144/1354-079309-903

Péron-Pinvidic, G., L. Gernigon, C. Gaina, P. Ball, 2012a. Insights from the Jan Mayen system in the Norwegian–Greenland sea - I. Mapping of a microcontinent. Geophysical Journal International 191, 385-412, doi: 10.1111/j.1365-246X.2012.05639.x

Péron-Pinvidic, G., L. Gernigon, C. Gaina, P. Ball, 2012b. Insights from the Jan Mayen system in the Norwegian-Greenland Sea - II. Architecture of a microcontinent. Geophysical Journal International 191, 413–435, doi: 10.1111/j.1365-246X.2012.05623.x

Péron-Pinvidic, G., G. Manatschal, P. T. Osmundsen, 2013. Structural comparison of archetypal Atlantic rifted margins: A review of observations and concepts. Marine and Petroleum Geology, 43, 21–47, doi: 10.1016/j.marpetgeo.2013.02.002

Quinquis, M., S.J.H. Buiter, S. Ellis, 2011. The role of boundary conditions in numerical models of subduction zone dynamics. Tectonophysics 497, 57-70, doi:10.1016/j.tecto.2010.11.001

Quinquis, M.E.T., S.J.H. Buiter, 2014. Testing the effects of basic numerical implementations of water migration on models of subduction dynamics. Solid Earth 5, 537-555, doi: 10.5194/se-5-537-2014

Ranalli, G., 1987. Rheology of the Earth: Allen & Unwin Inc., USA. 366 pp.

Reiner, M., 1964. The Deborah number. Physics Today 62

Rice, J. R., 1992. Fault stress states, pore pressure distributions, and the weakness of the San Andreas fault. In Evans, B. and Wong, T., eds., Fault Mechanics and Transport Properties of Rocks, San Diego, California, 475– 503

Saunders, A.D., J.G. Fitton, A.C. Kerr, M.J. Norry, R.W. Kent, 1997. The North Atlantic igneous province. In Mahoney, J.J., Coffin, M.F., eds., Large Igneous Provinces: Continental, Oceanic, and Planetary Flood Volcanism. Geophysical Monograph, 100. AGU, 45–93

Schellart, W.P., G.S. Lister, V.G. Toy, 2006. A Late Cretaceous and Cenozoic reconstruction of the Southwest Pacific region: Tectonics controlled by subduction and slab rollback processes. Earth-Science Reviews 76, 191-233, doi: 10.1016/j.earscirev.2006.01.002

Schenk, O., K. Gärtner, 2004. Solving unsymmetric sparse systems of linear equations with PARDISO. Future Generation Computer Systems 20, 475–487, doi: 10.1016/j.future.2003.07.011

Schmeling, H., 2000, Partial melting and melt segregation in a convecting mantle. In N. Bagdassarov, D. Laporte, A.B. Thompson, eds., Physics and chemistry of partially molten rocks 11, 141–178, Springer Netherlands

Schmeling, H., 2010. Crustal accretion at high temperature spreading centres: Rheological control of crustal thickness. Physics of the Earth and Planetary Interiors 183, 447–455, doi: 10.1016/j.pepi.2010.10.004.

Schutt, D. L, C.E. Lesher, 2006. Effects of melt depletion on the density and seismic velocity of garnet and spinel lherzolite. Journal of Geophysical Research 111, B05401, doi: 10.1029/2003JB002950.

Scott, D. R., D.J. Stevenson, 1989. A self-consistent model of melting, magma migration and buoyancy-driven circulation beneath mid-ocean ridges. Journal of Geophysical Research 94, 2973–2988, doi: 10.1029/JB094iB03p02973

Scrutton, R.A., 1966. Microcontinents and their significance. In Drake, C.L., ed., Geodynamics: Progress and Prospects, American Geophysical Union, Washington, D.C., 177-189

Sdrolias, M., R. Müller, C. Gaina, 2003. Tectonic evolution of the southwest Pacific using constraints from backarc basins. In R. Hillis, R. Müller, eds., Evolution and dynamics of the Australian plate, GSA Special Paper 372, 343–359, Geological Society of America

Shannon, P. M., 1991. The development of Irish offshore sedimentary basins. Journal of the Geological Society 148, 181–189, doi: 10.1144/gsjgs.148.1.0181

Sleep, N.H., 1997. Lateral flow and ponding of starting plume material. Journal of Geophysical Research 102, 10,001-10,012

Spiegelman, M., D. McKenzie, 1987. Simple 2-D models for melt extraction at mid-ocean ridges and island arcs. Earth and Planetary Science Letters 83, 137–152, doi: 10.1016/0012-821X(87)90057-4

Storey, M., R.A. Duncan, C. Tegner, 2007. Timing and duration of volcanism in the North Atlantic Igneous Province: implications for geodynamics and links to the Iceland hotspot. Chemical Geology 241, 264–281, doi: 10.1016/j.chemgeo. 2007.01.016

Stratford, W., H. Thybo, J.I. Faleide, O. Olesen, A. Tryggvason, 2009. New Moho Map for onshore southern Norway. Geophysical Journal International 178, 1755-1765.

Talwani, M., O. Eldholm, 1977. Evolution of the Norwegian-Greenland Sea. Geological Society of America Bulletin 88, 969-999

Tetreault, J.L., S.J.H. Buiter, 2012. Geodynamic models of terrane accretion: Testing the fate of island arcs, oceanic plateaus, and continental fragments in subduction zones. Journal of Geophysical Research 117, B08403, doi: 10.1029/2012JB009316

Tetreault, J.L., S.J.H. Buiter, 2013. Why is it so difficult to create a microcontinent? Geological Society of Norway Winter Meeting, 8-10 January, Oslo.

Tetreault, J.L., S.J.H. Buiter, 2014. Future accreted terranes: a compilation of island arcs, oceanic plateaus, submarine ridges, seamounts, and continental fragments. Solid Earth 5, 1243-1275, doi: 10.5194/se-5-1243-2014

Tetreault, J.L., S.J.H. Buiter, 2015. Crustal structure of continental fragments. NGU report 2015.018

Tetreault, J.L., S.J.H. Buiter, The influence of extension rate and crustal rheology on the evolution of passive margins from rifting to break-up, in prep.

Todal, A., O. Edholm, 1998. Continental margin off Western India and Deccan Large Igneous Province. Marine Geophysical Researches 20, 273–291

Torsvik, T.H., L.M.R. Cocks, 2005. Norway in space and time: a centennial cavalcade. Norwegian Journal of Geology 85, 73–86

Torsvik, T.H., H.E.F. Amundsen, R.G. Trønnes, P.V. Doubrovine, C. Gaina, N.J. Kusznir, B. Steinberger, F. Corfu, L.D. Ashwal, W.L. Griffin, S.C. Werner, B. Jamtveit, 2015. Continental crust beneath southeast Iceland. Proceedings of the National Acedemy of Sciences of the United States of America, doi/10.1073/pnas.1423099112

van den Berg, A.P. , P.E. van Keken, D.A. Yuen, 1993. The effects of a composite non-Newtonian and Newtonian rheology on mantle convection. Geophysical Journal International 115(1), 62–78

Vogt, P.R., G.L. Johnson, L. Kristjansson, 1980. Morphology and Magnetic Anomalies North of Iceland. Journal of Geophysics 47, 67-80

White, R., D. McKenzie, 1989. Magmatism at rift zones: the generation of volcanic continental margins and flood basalts. Journal of Geophysical Research 94, 7685–7729

Yamasaki, T., L. Gernigon, 2010. Redistribution of the lithosphere deformation by the emplacement of underplated mafic bodies: implications for microcontinent formation. Journal of the Geological Society London 167, 961-971, doi: 10.1144/0016-76492010-027

Yatheesh, V., G.C. Bhattacharya, J. Dyment, 2009. Early oceanic opening off Western India–Pakistan margin: the Gop Basin revisited. Earth and Planetary Science Letters 284, 399–408, doi: 10.1016/j.epsl.2009.04.044

Zhou, Y., E. Rybacki, R. Wirth, C. He, G. Dresen, 2012. Creep of partially molten fine-grained gabbro under dry conditions. Journal of Geophysical Research 117, B05204, doi: 10.1029/2011JB008646

Zienkiewicz, O.C., R.L. Taylor, 2000. The Finite Element Method, Volume 1: The Basis, Fifth Edition, Butterworth-Heinemann, 689 pp.